AGU PUBLICATIONS

JGR

Journal of Geophysical Research: Atmospheres

RESEARCH ARTICLE

10.1002/2014JD022350

Key Points:
- Light-absorbing particles were measured at 67 central North American sites
- Sources of snow particulate absorption were soil, biomass burning, and pollution
- Great Plains snow in North America is cleaner than in the Great Plains of China

Supporting Information:
- Readme
- Figures S1–S5
- Tables S1 and S2

Correspondence to:
S. J. Doherty,
sarahd@atmos.washington.edu

Citation:
Doherty, S. J., C. Dang, D. A. Hegg, R. Zhang, and S. G. Warren (2014), Black carbon and other light-absorbing particles in snow of central North America, *J. Geophys. Res. Atmos.*, *119*, 12,807–12,831, doi:10.1002/2014JD022350.

Received 10 AUG 2014
Accepted 23 OCT 2014
Accepted article online 28 OCT 2014
Published online 25 NOV 2014
Corrected 5 MAY 2016

This article was corrected on 5 MAY 2016. See the end of the full text for details.

Black carbon and other light-absorbing particles in snow of central North America

Sarah J. Doherty[1], Cheng Dang[2], Dean A. Hegg[2], Rudong Zhang[2,3], and Stephen G. Warren[2]

[1]Joint Institute for the Study of Atmosphere and Ocean, Seattle, Washington, USA, [2]Department of Atmospheric Sciences, University of Washington, Seattle, Washington, USA, [3]Key Laboratory for Semi-Arid Climate Change of the Ministry of Education, College of Atmospheric Sciences, Lanzhou University, Lanzhou, China

Abstract Vertical profiles of light-absorbing particles in seasonal snow were sampled from 67 North American sites. Over 500 snow samples and 55 soil samples from these sites were optically analyzed for spectrally resolved visible light absorption. The optical measurements were used to estimate black carbon (BC) mixing ratios in snow (C_{BC}^{est}), contributions to absorption by BC and non-BC particles, and the absorption Ångström exponent of particles in snow and local soil. Sites in Canada tended to have the lowest BC mixing ratios (typically ~5–35 ng g^{-1}), with somewhat higher C_{BC}^{est} in the Pacific Northwest (typically ~5–40 ng g^{-1}) and Intramountain Northwest (typically 10–50 ng g^{-1}). The Northern U.S. Plains sites were the dirtiest, with C_{BC}^{est} typically ~15–70 ng g^{-1} and multiple sample layers with >100 ng g^{-1} BC in snow. Snow water samples were also chemically analyzed for standard anions, selected carbohydrates, and various elements. The chemical and optical data were input to a Positive Matrix Factorization analysis of the sources of particulate light absorption. These were soil, biomass/biofuel burning, and fossil fuel pollution. Comparable analyses have been conducted for the Arctic and North China, providing a broad, internally consistent data set. As in North China, soil is a significant contributor to snow particulate light absorption in the Great Plains. We also examine the concentrations and sources of snow particulate light absorption across a latitudinal transect from the northern U.S. Great Plains to Arctic Canada by combining the current data with our earlier Arctic survey.

1. Introduction

Model studies indicate that black carbon (BC) in snow may be responsible for a significant fraction of Northern Hemisphere warming in recent decades. BC lowers snow's very high albedo and triggers positive feedback processes, causing further reduction of surface albedo [e.g., *Flanner et al.*, 2007, 2009; *Bond et al.*, 2013]. Large-area surveys of BC in snow have been conducted in the Arctic and across northern China [*Clarke and Noone*, 1985; *Doherty et al.*, 2010; *Huang et al.*, 2011; *Wang et al.*, 2013; *Ye et al.*, 2012]. Regional median BC content from these surveys varies from 3 ng g^{-1} in Greenland to 1220 ng g^{-1} in northeast China. Here we present a survey in North America, using the same measurement and analysis techniques applied in the Arctic and North China surveys.

The previous northern China survey and the North American survey presented herein were motivated by the potentially large forcing by BC in snow in these regions. Both north China and central North America have large open plains regions. Darkened snow in these regions, where vegetation does not mask the snowpack, can affect the Earth's albedo more than in the boreal forest, where the snow is deeper and lasts longer but is largely hidden below trees. Another reason for regionally and seasonally significant radiative forcing due to BC in snow at middle latitudes is that the snow is closer to BC sources, with impacts on timing and rate of snowmelt. Snow darkening at high latitudes may not reduce springtime snow cover as much as at midlatitudes because at high latitudes the snow remains too cold to melt. At midlatitudes the temperatures are sufficiently warm that the addition of BC to the snowpack can push it to its melt point, triggering the snow albedo feedback [*Flanner et al.*, 2009]. Indeed, a regional model study investigating the impact of snow BC specifically on the hydrology of the western U.S. [*Qian et al.*, 2009] found that in most areas snow water runoff increased in February, which led to a diminished March snowpack with less runoff. While such model studies provide compelling results, they need to be tested for, among other things, accurate representation of snow BC mixing ratios and the sources and roles of other (non-BC) light-absorbing aerosol. In the north China survey, dust was found to be a large contributor to snow particulate absorption [*Wang et al.*, 2013]. This reduces BC's importance in lowering snow albedo (and therefore its radiative forcing). Of interest is whether non-BC absorbers also make a significant contribution to snow particulate absorption in the northern U.S.

©2014. American Geophysical Union. All Rights Reserved.

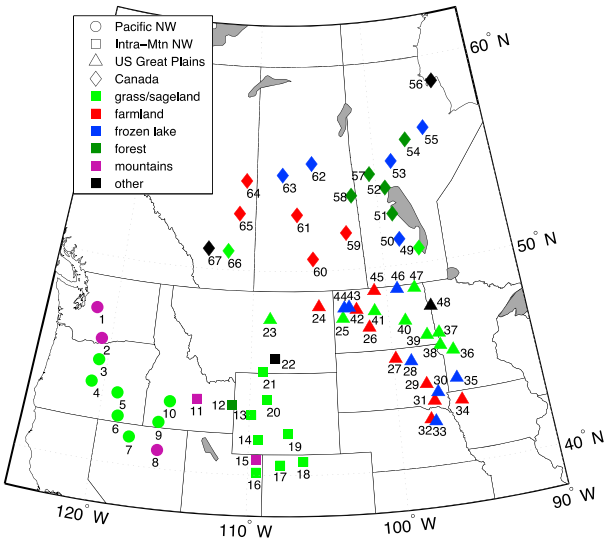

Figure 1. Snow sampling locations, site numbers, and regional groupings. See Table S1 for sampling dates and latitude/longitude coordinates of each site. Sample region is indicated by symbol shape, and the land surface type of the sampling site is indicated by the color of the site symbol, as shown in the legend. Sites 22, 48, and 67 ("other") include samples near or in urban areas, as well as sites in farmland. Site 56 is on boreal tundra. Note that the attribution of surface type is not exact. For example, some sites are on a lake but surrounded by farmland (e.g., sites 28, 30, 33, and 35), on a lake but surrounded by forest (e.g., sites 53, 55, and 62), in the forest and in the mountains (sites 1 and 2), or in sage or grasslands and in the mountains (e.g., sites 8 and 11). (See also Table S1 and Figure S1.)

A snowpack that has not yet started to melt holds a deposition record over the accumulation season. Vertically resolved snowpack particulate mixing ratios therefore provide information on how the types and mixing ratios of light-absorbing particles evolve with the snowfall season. In addition, mixing ratio profiles provide some insight to atmospheric aerosol deposition rates. Model-model and model-measurement comparisons indicate that one of the largest sources of uncertainty in atmospheric BC distributions is the rate of BC deposition [*Koch et al.*, 2009a; *Schwarz et al.*, 2010; *Garrett et al.*, 2010]. The scale of these uncertainties is such that even coarse metrics such as an estimate of the total mass of BC deposited over the winter season may be useful for constraining models.

Previous large-area surveys in the Arctic [*Doherty et al.*, 2010] and northern China [*Wang et al.*, 2013] used an Integrating Sphere integrating SandWich (ISSW) spectrophotometer [*Grenfell et al.*, 2011] to measure BC and other insoluble light-absorbing particles in snow. Here we present the results of a similar survey of seasonal snow in 13 American states and three Canadian Provinces (Figure 1). As in the previous studies of *Doherty et al.* [2010] and *Wang et al.* [2013], the ISSW measurements were used to determine the maximum possible BC mixing ratio in snow and the particulate light absorption Ångström exponent (*Å*), which relates to the type of particles (e.g., from fossil fuel burning, biomass burning, and mineral dust). The measurements are also used to estimate the actual BC mixing ratio in snow and the fraction of sunlight absorption in snow due to BC versus non-BC light-absorbing particles. A subset of the snow samples were chemically analyzed to determine the sources of the BC and other light-absorbing particles in snow via Positive Matrix Factorization (PMF) analysis, following *Hegg et al.* [2009, 2010] and *Zhang et al.* [2013].

2. Methods

2.1. Sample Collection and Filtration

Snow samples were gathered 10 January (site 1) and 28 January through 21 March 2013 (sites 2–67), starting in the U.S. Pacific Northwest, then through the Rocky Mountains, the northern U.S. Great Plains, and the Canadian Great Plains and boreal forests (Figure 1 and Table S1 in the supporting information). Ideally, samples would have been gathered at all sites (a) at the peak of snow depth, but before significant snowmelt, (b) in locations with only a small influence from very local sources, and (c) on a common land type (e.g., farmland and grasslands). Since this was logistically not possible, we tried to time the 2 month campaign so that the early sites were sampled as late as possible without risking being too far into the spring melt season at the last sites. As discussed below, with a couple of intentional exceptions, efforts were made to sample away from local sources and in open areas so that detritus from trees and bushes did not contaminate the snow, as this would make it difficult to isolate the effects of deposited aerosols.

Samples were gathered at vertical intervals, usually through the entire snowpack, at each site. Sampling vertical resolution varied from about 2 cm to 10 cm and was typically 4–5 cm. Sample layer selection was dictated by total snow depth and the identification of visibly distinct changes in snow type, such as new

©2014. American Geophysical Union. All Rights Reserved.

Figure 2. Pictures of several snow sampling sites: (a) Site 3, Colorado shrub/open area; (b) Site 15, Utah mountain area; (c) Site 23, Montana grass/shrubland, melting snow; (d) Site 27, South Dakota farmland, shallow snow and strong wind; picture shows the snow drift sampled; (e) Site 31, South Dakota farmland; (f) Site 44, on Lake Sakakawea, North Dakota; (g) Site 52, Manitoba, opening in forested area; and (h) Site 61, on Saskatchewan farmland.

snow, crust, and depth hoar [*LaChapelle*, 1969]. Sites were selected to be roughly 160 km apart, with allowances for snow cover, terrain and accessibility to potential sampling sites. To minimize the impact of pollution from very local transportation, snow samples were usually gathered about 1 km or more, nominally upwind, from the approach road, which usually was not a major highway. Photographs of some of the sites are shown in Figure 2. At most sites, soil samples were also collected for optical analysis of their spectral light absorption.

©2014. American Geophysical Union. All Rights Reserved.

Snow particle concentrations and composition depend on dry and wet deposition of particles from the atmosphere, but also on in-snow processes. Sublimation and melting amplify snow concentrations [e.g., *Flanner et al*., 2007; *Doherty et al*., 2010; *Xu et al*., 2012]. Redistribution of water within the snowpack, such as with the formation of depth hoar, also affects snow particle mixing ratios. In windy areas with thin/patchy snow, local soil can readily be lofted and deposited to the snow or mixed with falling snow on very small spatial scales. In climate models, most particle deposition to snow at the global scale is through wet deposition (e.g., ~70% to >90% of total deposited BC in the models of *Flanner et al*. [2007], *Koch et al*. [2009b], and *Jacobson* [2004]). However, global models likely do not capture subgrid-scale lofting and dry deposition of soil with near-surface winds. Based on our visual observations in the field, and the results discussed below, we argue that this process has a significant influence on total snow particle light absorption in some regions. Noting the importance of these processes, we recorded total snow depth, snow type in each sample layer, and the vertically resolved snow density at each site.

Based on the surface land type and seasonal-average snow water equivalent (Figures S1 and S2), the 67 sites are grouped into four regions (Figure 1). In addition, we indicate in Figure 1 the general surface type at the sampling site.

Sites 1 to 10 are in the Pacific Northwest, bounded by the Pacific Ocean and the Rocky Mountains. In this region, the snow depth is mainly influenced by elevation. Most of these sites were located at moderately high elevation (approximately 800–2000 m; Table S1) and were often on grazing land dominated by grass or sagebrush vegetation; some were at mountain passes.

Sites 11 to 22 are in the Rocky Mountain area, which we will refer to as the Intramountain Northwest. Most of these sites are located at approximately 2000 ± 500 m elevation (Table S1), in sage/grasslands, forests, and mountainous areas. Snow was more consistently deep than in the Pacific Northwest, and there was continuous snow cover from January to March. An exception is site 22, which is actually six closely spaced sites east of Billings, Montana. Here the snow cover was transient: Our interest was in gathering samples of fresh snow that fell on mostly bare ground at a range of distances from Billings.

Sites 23 to 48 are in the Northern U.S. Plains, primarily in the Dakotas. This region is mostly farmland, with small wildlife preserves containing lakes and grasslands. Most sites are at ~200–700 m elevation, and there is much less site-to-site variation in elevation than in the Pacific Northwest or Intramountain Northwest. Of special interest are the effects of the rapidly growing Bakken oil fields in the northwest of North Dakota, near sites 25 and 42–44. During the sampling period, the snow at sites 23 and 32–35 was patchy; therefore, snow samples were collected where the snow was locally deeper, in drifts. By contrast, snow at sites 36 to 48 was deeper and more continuous. Site 48 is on farmland on the outskirts of Grand Forks, North Dakota. Here we sampled only the newly fallen snow during a snowfall event, at three locations. The first (48A) was outside our hotel in Grand Forks; the next two were about 20 km southeast of Grand Forks and were separated from each other by about 20 m, one on farmland next to a river (48B) and the other on the frozen river (48C). New snow accumulation was deeper on the river (~20 cm) than on the farmland or in town (~10 cm), likely because it was sheltered from the wind by the riverbanks.

Sites 49 to 67 are all in Canada, and at all but site 67 (east of Calgary), the snow depth was at least 20 cm. The snow in this region (the Prairie Provinces: Manitoba, Saskatchewan, and Alberta) is deeper than at the locations we sampled in the U.S. Sites 49–58 were at <300 m elevation (Table S1); then elevation generally increased moving west and south from site 58, to approximately 1000 m at site 67 east of Calgary.

Sites 49 to 56 follow roughly a south-to-north transect from the U.S. border to our northernmost site at Churchill, Manitoba. The southwesternmost eight Canadian sites (sites 59–61 and 65–67) are within the Great Plains. The remaining Canadian sites are in general within the boreal forest area, either in a gap between trees or on a frozen lake. An exception is Site 56, at <20 m elevation at the forest-tundra boundary by the shore of Hudson Bay. Site 67 is actually three sites, all on farmland, sampled as we approached Calgary from the east/southeast. The sites are approximately 60 km (67A), 45 km (67B), and 30 km (67C) from edge of the Calgary city limits.

At each site, snow samples were collected in two side-by-side vertical columns, allowing for comparison and averaging of sample pairs. One column's samples were gathered in glass jars manufactured by I-CHEM, precleaned to Environmental Protection Agency (EPA) level II specifications (available through VWR; www.vwr.com)

©2014. American Geophysical Union. All Rights Reserved.

so that the meltwater could be used for chemical analysis. Teflon-lined lids were used for all glass jars. Some jars were reused to collect samples for optical (ISSW) analysis only, but they first were cleaned with methanol then rinsed at least twice with distilled water. At most sites one surface and one subsurface sample were collected for both optical and chemical analysis; all of these were gathered in new precleaned jars.

Glass jars are advantageous because they do not suffer from the artifacts identified in previous studies when samples were gathered in plastic bags—e.g., having particles stick to the plastic [*Doherty et al*., 2010; *Wang et al*., 2013]. However, gathering two full profiles in glass jars is not practical in large-area surveys, so samples from the second column were gathered in food-grade plastic bags. The food-grade bags were selected after testing a variety of sampling containers (glass jars and several types of plastic bags). No systematic difference was found between samples gathered in clean glass jars and those gathered in the food-grade bags. For site 56 (at Churchill on Hudson Bay, which we reached by train), use of glass jars was not logistically feasible, so both sample profiles were collected in food-grade bags.

Nominally, sample profiles reflect the typical state of the snowpack in the region of the sampling site, and we are able to gather samples from multiple layers. However, at several sites, the snow was so thin that only one layer of snow could be sampled. For places where the snow was patchy and/or where the snow distribution appears to be heavily influenced by winds, by necessity we collected snow from a drift. In this case sample depth likely does not correlate well with snow/particle deposition time.

All snow samples were kept frozen until being processed in temporary laboratories set up in hotel rooms every 3 to 4 days. For samples collected in bags, snow was spooned into a clean glass beaker with a clean stainless steel utensil and then melted rapidly in a microwave oven. Samples collected with glass jars were melted directly in the jars in the microwave. A clean plastic bag or a jar lid was used to cover the container during melting to prevent contamination. To reduce the loss of particles to container walls, melted snow was immediately drawn through Nuclepore filters of 0.4 μm pore size after any very coarse biological particles (e.g., grass and leaves) were removed using a clean stainless steel spoon. At most sites, portions of the melted snow from one surface sample and one subsurface sample were saved in 100 mL I-CHEM glass jars precleaned to EPA level II specifications for later chemical analysis. In some cases filtrate from the 0.4 μm nuclepore filters was also saved. One to two drops of chloroform were added to snow meltwater samples to prevent biological growth; they were then immediately refrozen and kept frozen until they could be chemically analyzed in the lab.

As discussed in previous studies [*Doherty et al*., 2010; *Wang et al*., 2013], the 0.4 μm nuclepore filters do not have 100% capture efficiency of all particles, although most particles down to 0.2 μm diameter will be captured. We do not use filters with a smaller pore size for normal processing because the flow rate is prohibitively slow. Capture efficiency of the 0.4 μm filters was quantified by running 16 of the nuclepore samples' filtrate through 0.2 μm nuclepore filters then comparing the optical absorption on the filter pairs. Additional tests running the 0.2 μm filtrate through 0.1 μm filters found zero undercatch for the 0.2 μm filters. In previous studies, the undercatch rate was typically 15% but varied from 0 to 40% [*Doherty et al*., 2010; *Wang et al*., 2013]. However, in this field campaign, the undercatch rate was lower, 0–10%. Therefore, all concentration-dependent parameters from the ISSW analysis presented here have a 5% undercatch correction applied.

2.2. Optical Analysis

To quantify the spectral light absorption due to particles in snow, we use a modified version of the ISSW spectrophotometer described by *Grenfell et al*. [2011] to analyze the filters. This instrument uses the diffuse radiation field from an integrating sphere to illuminate the filter from below, and transmission through the filter is measured with a spectrometer. In the modified ISSW, the "integrating sandwich diffuser" located above the sample filter (see Figure 2 of *Grenfell et al*. [2011]) has been replaced with a second integrating sphere. Thus, the sample filter is now sandwiched between two integrating spheres. Fiber optics feed light into the lower sphere via a side port and transmit light out of a side port in the upper sphere to the spectrometer. Baffles block direct illumination from reaching the filter in the lower sphere and block direct "viewing" of the filter by the spectrometer from the upper sphere. Because the loaded filter is suspended between two integrating spheres, nominally the only loss of light is due to absorption by particles on the filter. The light source/spectrometer combination has sufficient signal-to-noise to measure spectrally resolved signal attenuation over the wavelength range 450–750 nm at 1 nm resolution, which we average to 10 nm resolution.

©2014. American Geophysical Union. All Rights Reserved.

The maximum possible loading of BC on the filters is calculated by assuming that all the absorption at 650–700 nm is due to BC. The spectrum of light attenuation is converted to an equivalent BC mass loading using a set of nuclepore filters with a range of known (weighed) loadings of fullerene (Alfa Aesar, Inc., Ward Hill, MA, USA), a synthetic BC. As described in detail by *Grenfell et al.* [2011], the synthetic BC standards are used to generate calibration curves of BC-equivalent loading versus attenuation for each 10 nm wide wavelength band. Calibration uncertainty at most filter loadings is <10% [see *Grenfell et al.*, 2011, Figures 3–5, and associated discussion]. The resulting BC-equivalent loading quantifies the mass of fullerene needed to produce the same amount of light absorption within a given wavelength range as that of all particles on the sample filter. The fullerene-equivalent loading ($\mu g\,cm^{-2}$) is converted to a maximum possible snow BC mixing ratio, C_{BC}^{max}, by multiplying by the filter exposed area and dividing by the volume of snow water filtered.

Spectrally resolved absorption optical depth, $\tau_{abs}(\lambda)$, is given by multiplying the fullerene-equivalent loading by the estimated spectral mass absorption coefficient (MAC) of fullerene, which is 8.9, 7.2, and 6.5 $m^2\,g^{-1}$ at 450, 550, and 600 nm, respectively (absorption Ångström exponent of 1.1). This is similar to the MAC of atmospheric BC recommended by *Bond and Bergstrom* [2006] for bare BC, though BC in snow may have a different MAC than that in the atmosphere [*Schwarz et al.*, 2013]. A BC MAC of 7.2 $m^2\,g^{-1}$ at 550 nm is also similar to the 6.6 to 8 $m^2\,g^{-1}$ used in an earlier study of BC in snow by *Clarke and Noone* [1985].

The resulting spectrally resolved absorption is used to calculate the absorption Ångström exponent of all particles on the filter ($Å_{tot}$), where

$$Å_{tot} = -\frac{\ln[\tau_{abs}(\lambda_1)/\tau_{abs}(\lambda_2)]}{\ln(\lambda_1/\lambda_2)}. \quad (1)$$

Note that all values of the absorption Ångström exponent discussed herein are defined for $\lambda_1 = 450$ nm and $\lambda_2 = 600$ nm.

Climate model studies have focused on the effect of snow albedo reduction by BC specifically, so it is of interest to estimate the mixing ratio of BC in our samples. To separate the absorption contribution from BC versus non-BC particles, we make use of differences in the wavelength dependence of their absorption. The absorption Ångström exponent of all particles on our filters ($Å_{tot}$) is due to a mix of BC and non-BC absorbers and so is intermediate between the values for BC ($Å_{BC}$) and non-BC ($Å_{non\text{-}BC}$) components. Absorption is apportioned by selecting values of $Å_{BC}$ and $Å_{non\text{-}BC}$ and assuming the two contribute to $Å_{tot}$ in proportion to their relative contributions to total absorption. For the Arctic survey, *Doherty et al.* [2010] assumed $Å_{BC} = 1$ and $Å_{non\text{-}BC} = 5$. The latter is considered an appropriate value for brown carbon from combustion [see *Doherty et al.*, 2010, and references therein] but is nonetheless highly uncertain [e.g., see *Doherty et al.*, 2010, Figure 16]. In the Arctic, assuming that non-BC absorption was mostly from combustion organics is consistent with the indication from chemical, PMF, and back trajectory analyses that most of the absorbing particles in Arctic snow were from either biomass/biofuel burning or fossil fuel pollution [*Hegg et al.*, 2009, 2010]. Snow samples from the north China survey, however, often had significant amounts of soil and mineral dust [*Zhang et al.*, 2013], so site-specific values of $Å_{non\text{-}BC}$ were used, based on the relative contributions of soil and combustion particles [*Wang et al.*, 2013].

For the North American samples, it was visibly obvious that local soil contributed significantly to total snow particulate light absorption in some locations. In particular, in the north-central U.S. Great Plains (sites 24–48), snowfall was often accompanied by strong winds. Most of this region is agricultural fields; some tilled. The combination of winds and exposed soil means that the local soil readily mixes with snow. During our sampling in this region, it was almost always windy, and soil from the fields could sometimes be seen blowing with the snow near the surface. Based on this observation, we assume that $Å_{non\text{-}BC}$ for our North American sites is determined by contributions from local soil and combustion organics. We assume that there is not a significant contribution from distant sources of mineral dust or soil. This is likely accurate for all sites except perhaps sites 13–20 (Utah/Wyoming/Colorado), where deserts in the region may contribute mineral dust. We also assume that soil samples we collected were representative of soil in that local area, though we cannot test the accuracy of this assumption.

As discussed below, a Positive Matrix Factorization (PMF) analysis indicates that three factors account for almost all of the light absorption by insoluble particles in our North American samples: soil, pollution,

©2014. American Geophysical Union. All Rights Reserved.

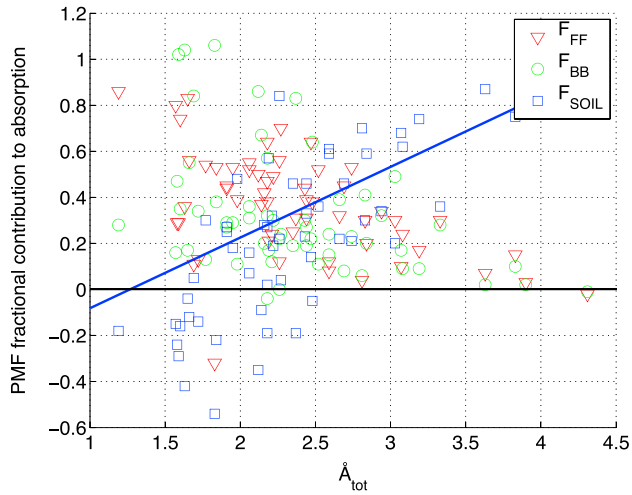

Figure 3. Correlation between PMF-determined fraction of absorption (C_{BC}^{max}) due to fossil-fuel pollution (F_{FF}), biomass burning (F_{BB}), and soil (F_{SOIL}) and $Å_{tot}$, for those samples that were analyzed both optically and chemically. Also shown is the weighted fit to F_{SOIL} versus. $Å_{tot}$ (blue line), as discussed in the text. This fit is used to apportion non-BC absorption to soil versus fossil + biomass burning brown carbon, based on each sample's $Å_{tot}$. The weighted fit is $F_{SOIL} = (0.307 \times Å_{tot} – 0.388)$ and has $r^2 = 0.50$.

and biomass burning (Figure S3). The PMF analysis also provides estimates of the fractional contributions (F_{SOIL}, F_{FF}, and F_{BB}) of each of these factors to the 650–700 nm absorption. The "pollution" factor includes fossil fuel combustion sources as well as other emissions from industrial processes, so it is not strictly a fossil fuel factor. However, the light-absorbing particles in the pollution factor are likely mostly BC and organic carbon from fossil fuel combustion (hence, "F_{FF}"). The biomass (BB) factor includes both open biomass burning and biofuel (e.g., woodstove burning), so this source factor includes both natural and anthropogenic emissions. (See sections 2.3 and 3.0 for more details.) Correlation of these three source factors against $Å_{tot}$ for paired optically/chemically analyzed samples (Figure 3) shows that changes in $Å_{tot}$ correlate significantly with changes in F_{SOIL}, but only weakly with changes in F_{FF} and F_{BB}. We leverage this correlation to use $Å_{tot}$ as a metric for the relative contributions of soil and combustion (i.e., brown carbon) to the non-BC absorption.

F_{SOIL} is, on average, negative at low $Å_{tot}$ (Figure 3), which is clearly unphysical. This is due in part to the fact that there is high variance in F_{SOIL} at low $Å_{tot}$. Thus, rather than do a straight correlation, we did a weighted fit to F_{SOIL} versus $Å_{tot}$. We calculated the variance in F_{SOIL} in four bands of $Å_{tot}$ (1.25–2.0, 2.0–2.75, 2.75–3.5, and 3.5–4.25), and weighted F_{SOIL} in each band by the inverse of the variance. We then calculated a fit (exponential) to the weights versus the bin-average $Å_{tot}$, and the fit was used to calculate a weight for each data point in Figure 3. A linear fit to the weighted data gives F_{SOIL} as a function of $Å_{tot}$ (blue line in Figure 3). The contribution to absorption by biomass and pollution combined is assumed to be $(1 - F_{SOIL})$. Where F_{SOIL} is negative, it is set to 0, so for $Å_{tot} < 1.26$, $F_{SOIL} = 0$; otherwise, $F_{SOIL} = 0.307 \times Å_{tot} – 0.388$. We then calculate

$$Å_{non\text{-}BC} = F_{SOIL} \times Å_{soil} + (1 - F_{SOIL}) \times Å_{OC}. \quad (2)$$

Consistent with *Doherty et al.* [2010], we assumed $Å_{OC} = 5.0$. $Å_{soil}$ is site-specific and, where available, is based on ISSW analysis of local soil samples.

Following *Wang et al.* [2013], soil samples were sonicated in milli-Q water, filtered through 0.4 μm nuclepore filters, and then analyzed with the ISSW spectrophotometer for $Å_{soil}$. In order to capture the range of particles that might be lofted in wind and deposited locally to the snow, very large grains or vegetation in the soil were removed from the soil/water solution (if they floated) or allowed to settle in the solution before filtering. Soil-loaded filters were then measured with the ISSW. Soil was collected at all but 12 sites (1, 4, 22, 27–31, 44, 48, and 66–67); for these sites, we interpolated $Å_{soil}$ based on adjacent sites (Figures 4 and 5 and Tables 2–6). Figure 5 shows, as a reference, how $Å_{tot}$, $Å_{soil}$, and $Å_{non\text{-}BC}$ compare for the subset of samples included in the PMF analysis. Note that while there is a single value of $Å_{soil}$ for each *site*, $Å_{tot}$, and therefore F_{SOIL} and $Å_{non\text{-}BC}$ vary for each *sample*.

Using these values of $Å_{non\text{-}BC}$, and setting $Å_{BC} = 1.1$, we apportion the 450–600 nm absorption to BC and non-BC constituents per *Grenfell et al.* [2011]. The fraction of absorption due to BC at shorter (down to 450 nm) and longer (up to 750 nm) wavelengths is extrapolated by again assuming $Å_{BC} = 1.1$. With the spectrally resolved absorption attributed to BC and non-BC components, we can estimate the mixing ratio of BC in snow, C_{BC}^{est}, and the fraction of sunlight absorbed by non-BC particles in the snow ($f_{non\text{-}BC}^{est}$). The latter is calculated by (1) extrapolating the absorption spectra linearly from 450 nm down to 300 nm [*Grenfell et al.*, 2011; *Doherty*

©2014. American Geophysical Union. All Rights Reserved.

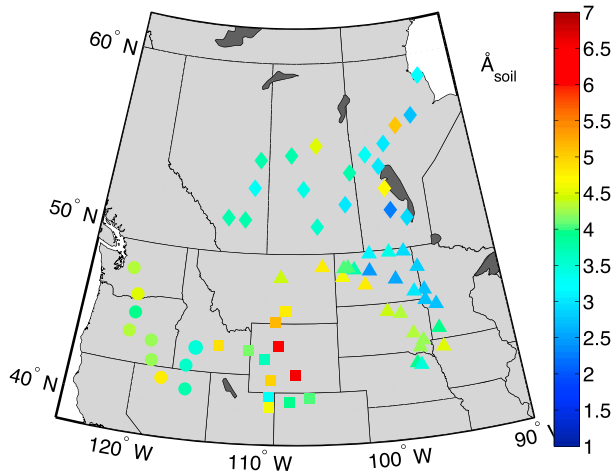

Figure 4. $Å_{soil}$ for each sampling site. For sites with no soil sample, $Å_{soil}$ is interpolated based on the values at geographically adjacent sites (Figure 5).

et al., 2010]; (2) weighting the non-BC absorption spectra and all-component (total) absorption spectra by a downwelling solar irradiance spectrum appropriate for clear-sky, midlatitude winter (see Figure 4 of *Wang et al.* [2013]); (3) integrating these weighted spectra across the visible range; and (4) taking the ratio of the two integrals. The sunlight-weighted total snow particulate absorption is also used to estimate the equivalent amount of BC that would be needed to account for the spectrally integrated absorption of sunlight by all particles in snow, C_{BC}^{equiv}. The quantity C_{BC}^{equiv} is always greater than C_{BC}^{max}, because absorption increases at shorter wavelengths more strongly for non-BC absorbers than for BC. We caution that C_{BC}^{equiv} should not be considered an estimate of the mixing ratio of BC in snow. Rather, it is a metric that can be used for, e.g., models of snow albedo that account for absorption by BC only (and not other particles) in snow, if one wishes to represent the integrated visible-band albedo reduction by all particles in snow.

In sum, we calculate the following quantities:

1. C_{BC}^{max} (ng g^{-1}): maximum possible snow BC mixing ratio
2. C_{BC}^{est} (ng g^{-1}): estimated snow BC mixing ratio
3. C_{BC}^{equiv} (ng g^{-1}): the amount of BC that would be needed to produce absorption of solar energy, integrated 300–750 nm, by all insoluble particles in snow
4. $Å_{tot}$: absorption Ångström exponent (450–600 nm) for all insoluble particles in snow
5. f_{NBC}^{est} (%): estimated fraction of solar energy absorption 300–750 nm due to insoluble, non-BC components of the particles in snow.

In items (3) and (5), the integration is limited to wavelengths 300–750 nm, because for $C_{BC}^{equiv} < 100$ ng g^{-1} the impurities in snow have little effect on snow albedo for $\lambda > 750$ nm (Figure 7 of *Warren and Wiscombe* [1980]). Note that when the fraction of 650–700 nm absorption due to BC is estimated to be less than 25% (which corresponds approximately to $f_{NBC}^{est} > 85\%$), we do not provide an estimate of the BC mixing ratio because it is considered too uncertain.

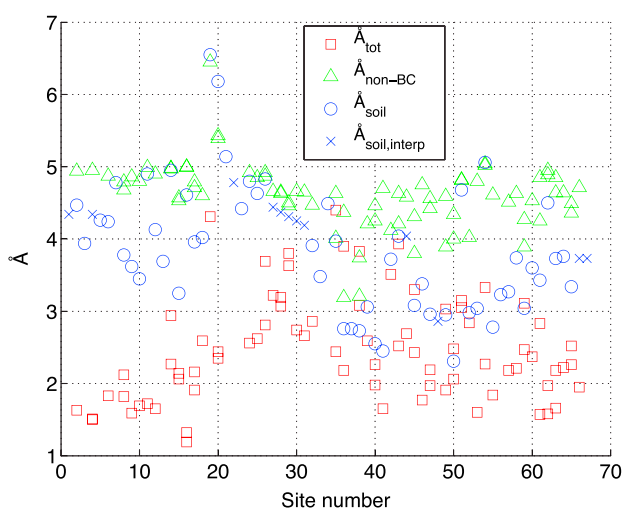

Figure 5. $Å_{tot}$, $Å_{soil}$, and $Å_{non\text{-}BC}$ for just those samples used in the PMF analysis (and shown in Figure 3).

We remind the reader that all mixing ratios (C_{BC}^{max}, C_{BC}^{est}, and C_{BC}^{equiv}) are derived from optical measurements of absorption that assume our calibration material (fullerene synthetic BC) has a mass absorption coefficient of 7.2 m^2 g^{-1} at 550 nm and an absorption Ångström exponent of 1.1. While this is close to the recommended value of 7.5 m^2 g^{-1} of *Bond and Bergstrom* [2006] for bare BC, the mass absorption coefficient of the BC in our snow samples may be higher or lower than this. Factors that affect BC MAC include whether or not

©2014. American Geophysical Union. All Rights Reserved.

it is coated with other materials and the size distribution of the BC. Coatings generally enhance BC MAC, as do smaller size distributions [*Bond et al*., 2013]. It appears that the sizes of BC particles in snow are larger than when they are in the atmosphere [*Schwarz et al*., 2012], so the MAC of bare BC in snow might be lower than that recommended for atmospheric BC. On the other hand, if there are very small particles containing BC in our samples, these may pass through our 0.4 μm filters, though our undercatch tests indicate that these account for only a small fraction of the absorption (<10%). It is not known to what degree BC in snow is internally mixed or coated with other constituents: BC that is incorporated into snow as components of cloud condensation nuclei may have lost soluble coatings in raindrop water, but BC-containing aerosols that are scavenged by falling snow may retain their original composition. Thus, BC in snow may in reality have a MAC that is either higher or lower than the assumed 5.6 $m^2 g^{-1}$ (at 650–700 nm). If it is, e.g., lower than this, the derived mass mixing ratios will be proportionately higher. In our previous study of BC in Arctic snow [*Doherty et al*., 2010], we used a different calibration material (M71), estimated to have a 650–700nm MAC of 5.0 $m^2 g^{-1}$. Thus, the values of C_{BC}^{max} and C_{BC}^{est} reported by *Doherty et al*. [2010] are 12% higher than they would be using the fullerene calibration standards used herein.

In addition to dependence on the assumed calibration material MAC, both C_{BC}^{est} and f_{NBC}^{est} depend on the selected values of $\mathring{A}_{BC}$ and $\mathring{A}_{non\text{-}BC}$, the latter of which is highly uncertain. Further, tests of the ISSW against gravimetrically determined filtered suspensions of synthetic BC (fullerene), a dust standard and mixes of the two, indicate some sensitivity to particulate scattering and high biases in derived BC mixing ratios in samples where BC is mixed with other components [*Schwarz et al*., 2012]. Based on this, we caution that C_{BC}^{est} may be biased high by as much as a factor of 2.5 for samples where f_{NBC}^{est} is greater than 50%; for f_{NBC}^{est} <50%, there may be a high bias on the order of 1.0–1.5.

2.3. Chemical Speciation and Factor Analysis

Both the chemical and factor (PMF) analyses applied here follow those of *Zhang et al*. [2013] for a survey of North China snow samples; details of the approach can be found therein. Briefly, snow water samples were melted and analyzed using ion chromatography with conductivity detection for standard ions, with both liquid chromatography-mass spectrometry and ion chromatography with pulsed amperometric detection (for carbohydrates), and with inductively coupled plasma-optical emission spectroscopy (ICP-MS; for various elements), per *Gao et al*. [2003]. Pairs of filtered and unfiltered snow water samples were compared to investigate the effect of filtering. These analyses yielded the mixing ratios in snow for the carbohydrates levoglucosan and mannitol, the ions formate, chloride, nitrate, the sum of succinate and malate (the two could not be resolved with the system utilized), sulfate and oxalate, and the elements Na, Al, Si, K, Ti, V, Cr, Mn, Fe, Ni, Cu, Zn, As, Cd, and Pb. From these, we estimate the concentrations of noncrustal manganese, vanadium, and potassium using Al as a crustal marker as in numerous previous studies [e.g., *Malm et al*., 1994; *Eldred et al*., 1997].

The chemically analyzed samples were also analyzed for the fraction of absorption due to organics via serial extractions using four organic solvents (methanol, dichloromethane, hexane, and sodium hydroxide), as described by *Dang and Hegg* [2014]. Particulate absorption ($\tau_{abs}(\lambda)$) was measured with the ISSW before extraction and after each extraction step. In this way, the visible absorption due to different organic groups was determined. Here we use OC_{abs} to denote the 470–700 nm absorption by all organics extracted by these four solvents. For a more detailed discussion of this analysis, see *Dang and Hegg* [2014].

The snow mixing ratios of the chemically analyzed constituents, along with C_{BC}^{max} and OC_{abs}, were input to a factor analysis to determine the sources of absorption by insoluble particles in the snow. The Positive Matrix Factorization receptor model used here (US EPA PMF 4.1; see *Paatero and Tapper* [1993, 2003] and *Paatero* [1997]) decomposes a matrix of speciated sample data into factor profiles that contain information on the chemical composition of each factor. It also provides the fractional contributions of each factor to the variance in an independent variable, in this case a measure of total particulate light absorption (C_{BC}^{max}). PMF accounts for measurement uncertainties and detection limits for each of the chemical concentrations and in C_{BC}^{max}; these are also input to the analyses. All but one of the former are estimated based on the analysis of replicate standards with uncertainties calculated as twice the standard error of the mean for each analyte species. The exception is the value for OC_{abs} derived from *Dang and Hegg* [2014] for which an uncertainty of 24% was used. For C_{BC}^{max}, the detection limit was 3 ppbm and the uncertainty 5% for the range of this data set (4.6% mean with a standard deviation of 3.6%) based on *Doherty et al*. [2010]. This 5% accounts for

©2014. American Geophysical Union. All Rights Reserved.

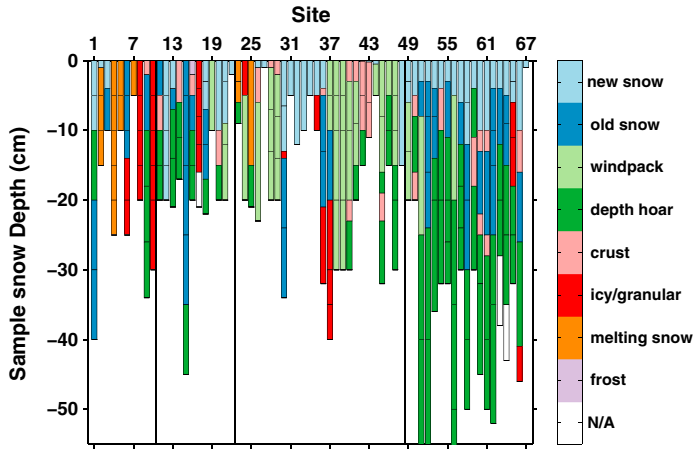

Figure 6. Vertical profiles showing snow type in sample layers. At Sites 51, 52, and 56, the total snow depth was 67 cm, 65 cm, and 100 cm, respectively; all snow below 55 cm was depth hoar. At Sites 56, we only sampled the snow to 65 cm depth. Vertical black lines demarcate the four sampling regions (Figure 1). See Table S1 for site locations and notes.

instrumental measurement uncertainty only. C_{BC}^{max} may, additionally, be biased by error in the spectral mass absorption efficiency of our fullerene standards, used to convert measured absorption to an equivalent BC mass. However, this source of error would apply uniformly across all values of C_{BC}^{max} in our data set. The PMF analysis results depend on correlating the variance in C_{BC}^{max} against that of other species and so would be unaffected by a uniform bias in the data set.

Factor profiles are determined fully by the PMF analysis, so source chemical "fingerprints" are not assumed a priori. Instead, the chemical combinations in each factor must be interpreted for what source type they best represent, taking into account, e.g., knowledge of likely emission sources in the region of interest. Normally PMF analysis is applied to a time series at an observation site; i.e., temporal variance is analyzed. Here as in some previous studies [i.e., *Paatero et al.*, 2003; *Chen et al.*, 2007; *Hegg et al.*, 2009, 2010; *Zhang et al.*, 2013], we use it to analyze spatial variance in source contributions.

The prognostic power of the PMF result is assessed by use of the parameter Q, essentially a modified χ^2 value quantifying the departure of predicted from observed values of the species concentrations input to the model. The model is run with varying numbers of factors/sources until a minimum Q value is achieved, taking into account the increase in the degrees of freedom implicit in increasing the number of factors in the solution [cf., *Reff et al.*, 2007].

3. Results

Snow type varied both geographically and with snow depth at a given site (Figure 6). At the earlier sites, several of our samples were of melting snow. In the U.S. Northern Great Plains (sites 23–48), most samples were of newly fallen or older wind-packed snow. At almost all of these sites, new snowfall was accompanied

Table 1. Regional Averages, Standard Deviations and, in Parentheses, Medians of Variables Estimated With the ISSW, for Surface and Subsurface Samples at Sites Within the Four Regions Shown in Figure 1[a]

	C_{BC}^{max}(ng g^{-1})	C_{BC}^{est}(ng g^{-1})	C_{BC}^{equiv}(ng g^{-1})	$Å_{tot}$	f_{NBC}^{est}(%)	$Å_{soil}$
			Pacific Northwest (Sites 1–10)			
Surface	38 ± 47 (24)	35 ± 44 (22)	43 ± 52 (29)	1.8 ± 0.2	22 ± 7	4.1 ± 0.4
Subsurface	37 ± 47 (27)	32 ± 30 (23)	46 ± 46 (34)	2.0 ± 0.2	29 ± 7	
			Intramountain Northwest (Sites 11–22)			
Surface	46 ± 47 (28)	37 ± 34 (24)	69 ± 93 (37)	2.1 ± 0.7	31 ± 15	4.7 ± 1.0
Subsurface	44 ± 46 (34)	27 ± 10 (29)	45 ± 23 (45)	2.3 ± 0.5	34 ± 11	
			Northern U.S. Plains (Sites 23–48)			
Surface	93 ± 125 (57)	44 ± 54 (30)	163 ± 245 (78)	2.7 ± 0.6	51 ± 17	3.7 ± 0.8
Subsurface	120 ± 134 (83)	78 ± 78 (47)	193 ± 226 (111)	2.7 ± 0.7	47 ± 16	
			Canada (Sites 49–67)			
Surface	27 ± 21 (18)	19 ± 13 (15)	40 ± 35 (25)	2.5 ± 0.4	47 ± 14	3.5 ± 0.7
Subsurface	25 ± 13 (22)	22 ± 11 (20)	32 ± 16 (28)	1.9 ± 0.2	29 ± 7	

[a]Medians for $Å_{tot}$ and f_{NBC}^{est} are not given because they differ insignificantly from the means.

©2014. American Geophysical Union. All Rights Reserved.

Table 2. Data for the Sites in the Pacific Northwest Region[a]

Site	Layer	Depth (cm)	C_{BC}^{max}	C_{BC}^{est}	C_{BC}^{equiv}	$\mathring{A}_{tot}$	$f_{non\text{-}BC}^{est}$	$\mathring{A}_{soil}$
1	surface (new)	0–5	12	10	14	1.92	28%	{4.34}
	subsurface (4)	5–40	7 ± 5	6 ± 4	9 ± 6	1.96 ± 0.08	28 ± 2%	
2	surface (new)	0–1	49	49	54	1.37	8%	4.47
	subsurface (3)	1–15	33 ± 17	32 ± 16	39 ± 19	1.64 ± 0.01	18 ± 0%	
3	surface (new)	0–4	24	23	29	1.79	22%	3.94
	subsurface (1)	4–10	30	26	40	2.16	35%	
4	surface (melting)	0–5	165	156	185	1.51	14%	{4.34}
	subsurface (1)	5–25	76 ± 55	72 ± 52	86 ± 61	1.59 ± 0.13	17 ± 4%	
5	surface (melting)	0–5	23	21	28	1.94	26%	4.26
	subsurface (1)	5–25	116	99	161	2.34	39%	
6	surface	0–5	5	4	6	1.83	25%	4.24
	subsurface (4)	5–25	9 ± 6	7 ± 4	13 ± 11	2.08 ± 0.43	33 ± 13%	
7	surface (melting)	0–5	39	35	50	2.05	30%	4.78
8	surface	0–5	32	29	38	1.82	24%	3.78
	subsurface (3)	5–20	17 ± 11	14 ± 8	23 ± 17	2.12 ± 0.28	36 ± 9%	
9	surface	0–2	14	13	16	1.59	17%	3.62
	subsurface (4)	2–34	14 ± 6	13 ± 6	17 ± 7	1.81 ± 0.13	24 ± 4%	
10	surface	0–5	13	11	15	1.69	21%	3.45
	subsurface (4)	5–30	18 ± 6	16 ± 6	21 ± 5	1.89 ± 0.25	26 ± 9%	
	all new snow	Drift	17	15	21	1.95	29%	
	all new snow	Drift	30	24	42	2.36	43%	

[a]Values are given for the surface layer, and averages and standard deviations for all layers below the surfacemost layer. Layers of new snowfall or of visibly melting snow are noted as such. The number of sample layers included in the subsurface is noted in parentheses; standard deviations are calculated only if three or more layers were sampled. Values of $\mathring{A}_{soil}$ interpolated from adjacent sites are given in curly brackets.

Table 3. As in Table 2, but for the Intramountain Northwest Sites

Site	Layer	Depth (cm)	C_{BC}^{max}	C_{BC}^{est}	C_{BC}^{equiv}	$\mathring{A}_{tot}$	$f_{non\text{-}BC}^{est}$	$\mathring{A}_{soil}$
11	surface	0–5	15	14	17	1.65	18%	4.90
	subsurface (3)	5–20	13 ± 2	12 ± 2	16 ± 2	1.86 ± 0.13	24 ± 4%	
12	surface (new)	0–5	20	18	22	1.65	18%	4.13
	subsurface (3; new)	5–20	18 ± 12	16 ± 12	20 ± 13	1.72 ± 0.17	21 ± 6%	
13	surface (new)	0–4	26	25	29	1.60	17%	3.69
	subsurface (3)	4–21	22 ± 15	20 ± 14	26 ± 18	1.83 ± 0.11	24 ± 4%	
14	surface (new)	0–6	169	147	230	2.27	36%	4.95
	subsurface (2)	6–17	177	40	380	2.86	51%	
15	surface	0–5	21	18	28	2.14	35%	3.25
	subsurface (4)	5–45	27 ± 10	23 ± 8	33 ± 14	1.96 ± 0.29	29 ± 9%	
16	surface	0–2	53	51	55	1.32	7%	4.61
	subsurface (4)	2–20	57 ± 42	42 ± 27	89 ± 75	2.55 ± 0.94	41 ± 25%	
17	surface	0–5	32	31	42	1.91	26%	3.96
	subsurface (3)	5–45	21 ± 9	19 ± 10	27 ± 9	2.13 ± 0.37	34 ± 14%	
18	surface	0–3	29	23	42	2.59	46%	4.02
	subsurface (4)	3–22	35 ± 10	29 ± 6	47 ± 19	2.19 ± 0.56	34 ± 17%	
19	snow drift 1	0–10	161	83	364	4.31	76%	6.55
	snow drift 2	0–10	37	29	62	3.26	54%	
20	surface (new)	0–6	23	21	31	2.35	33%	6.18
	subsurface (2)	6–17	34	30	45	2.28	33%	
21	surface	0–3	19	18	24	1.89	26%	5.14
	subsurface (3)	3–20	42 ± 12	36 ± 8	56 ± 20	2.18 ± 0.32	34 ± 9%	
22	surface	~0–5	45	39	59	2.20	34%	{4.78}
			40	35	53	2.19	33%	
			31	28	40	2.08	30%	
			27	24	35	2.09	30%	
			26	24	34	2.07	30%	
			23	21	30	2.02	28%	

©2014. American Geophysical Union. All Rights Reserved.

Table 4. As in Table 2, but for the Northern U.S. Plains Sites

Site	Layer	Depth (cm)	C_{BC}^{max}	C_{BC}^{est}	C_{BC}^{equiv}	$\mathring{A}_{tot}$	$f_{non\text{-}BC}^{est}$	$\mathring{A}_{soil}$
23	surface (new)	0–2	64	53	86	2.29	39%	4.42
	subsurface (2)	6–9	32	26	42	2.28	38%	
24	surface	0–4	65	51	94	2.56	46%	4.80
	subsurface (1)	4–20	24	21	33	2.28	37%	
25	surface	0–15	85	66	122	2.62	45%	4.63
	subsurface (1)	15–21	55	44	77	2.46	41%	
26	surface (new)	0–5	60	45	94	2.81	52%	4.83
	subsurface (2)	5–27	604	310	882	3.60	72%	
27	snow drift	0–10	522	295	952	3.22	65%	{4.45}
28	surface	0–1	74	47	128	3.19	63%	{4.37}
	subsurface (3)	1–20	48 ± 10	33 ± 2	79 ± 24	2.94 ± 0.44	55 ± 13%	
29	surface	0–2	132	47	267	3.80	82%	{4.31}
	subsurface (3)	2–20	103 ± 7	47 ± 3	203 ± 15	3.64 ± 0.01	77 ± 0%	
30	surface (new)	0–6.5	11	9	17	2.68	48%	{4.25}
	subsurface (4)	6.5–34	33 ± 18	25 ± 12	51 ± 29	2.73 ± 0.17	50 ± 5%	
31	all new snow	0–5	22	18	34	2.66	48%	{4.19}
32	all new snow	0–15	23	16	37	2.86	56%	3.91
33	all new snow	0–10	30	18	49	2.94	62%	3.48
34	all new snow	0–5	25	19	38	2.69	49%	4.49
35	surface (new)	0–5	39	31	54	2.44	43%	3.97
	subsurface (1)	5–10	294	—	718	4.40	~100%	
36	surface	0–6.5	7	6	10	2.18	38%	2.76
	subsurface (4)	6.5–34	227 ± 173	—	362 ± 199	3.12 ± 0.71	56 ± 27%	
37	surface	0–5	31	18	48	2.68	59%	2.76
	subsurface (5)	5–40	155 ± 167	162 ± 188	208 ± 195	2.49 ± 0.84	38 ± 26%	
38	surface	0–5	71	35	113	2.91	69%	2.73
	subsurface (3)	5–30	87 ± 44	34 ± 28	160 ± 110	3.17 ± 0.66	67 ± 23%	
39	surface	0–5	61	26	103	3.09	74%	3.06
	subsurface (3)	5–32	33 ± 13	17 ± 2	54 ± 25	2.84 ± 0.30	64 ± 13%	
40	surface	0–3	51	44	63	1.98	31%	2.55
	subsurface (4)	3–30	81 ± 64	66 ± 53	109 ± 89	2.20 ± 0.06	39 ± 2%	
41	surface	0–3	55	42	72	2.24	41%	2.45
	subsurface (3)	3–15	43 ± 29	38 ± 23	51 ± 38	1.67 ± 0.27	20 ± 10%	
42	surface (new)	0–0.5	192	61	356	3.51	83%	3.72
	subsurface (3)	0.5–15.5	168 ± 71	107 ± 32	262 ± 128	2.72 ± 0.39	54 ± 14%	
43	surface (new)	0–1	435	—	884	3.93	~100%	4.04
	subsurface (2)	1–11	100	71	147	2.60	49%	
44	surface (new)	0–0.5	297	—	598	3.88	~100%	{4.04}
	subsurface (1)	0.5–5.5	120	85	175	2.69	52%	
45	surface	0–8	73	25	127	3.23	81%	3.08
	subsurface (4)	8–32	46 ± 33	38 ± 29	59 ± 41	2.14 ± 0.20	36 ± 7%	
46	surface (new)	0–5	32	29	38	1.77	23%	3.38
	subsurface (2)	5–15	54	49	66	1.83	25%	
47	surface	0–5	31	26	42	2.19	39%	2.96
	subsurface (4)	5–30	86 ± 57	77 ± 52	113 ± 77	2.04 ± 0.05	32 ± 1%	
48	drifted new snow	~0–10	65	57	84	2.04	33%	{2.86}
		~0–10	33	29	42	1.94	29%	
		~0–20	21	19	26	1.83	26%	

by strong surface winds, so the newly fallen snow was also often wind packed. The snowpack in this region was often patchy, with sample snow depths in Figure 6 sometimes being the depth in a drift (see notes in Table S1). In the Northern Great Plains region, snow depth increased to the north and east; our sites follow the NW to SE diagonal through North and South Dakota that roughly demarks the transition from bare land to snow-covered land (Figure S2). Farther north, in Canada, winds were often calmer both during and between snowfall events, and the snowpack was deeper. Surface samples in Canada were all of snow that had fallen in the previous 1–3 days, and the deepest layers of the snowpack were usually depth hoar (as we also found in Arctic snow [*Doherty et al.*, 2010]). For many of the United States sites, snow cover is intermittent, even in

©2014. American Geophysical Union. All Rights Reserved.

Table 5. As in Table 2, but for the Canadian Sites

Site	Layer	Depth (cm)	C_{BC}^{max}	C_{BC}^{est}	C_{BC}^{equiv}	$\mathring{A}_{tot}$	$f_{non\text{-}BC}^{est}$	$\mathring{A}_{soil}$
49	surface (new)	0–3	14	8	21	2.76	61%	2.95
	subsurface (3)	3–20	45 ± 18	38 ± 17	57 ± 19	2.06 ± 0.29	34 ± 11%	
50	surface (new)	0–5	12	8	17	2.48	54%	2.31
	subsurface (3)	5–20	58 ± 46	52 ± 43	67 ± 49	1.81 ± 0.24	26 ± 8%	
51	surface (new)	0–3	94	60	154	3.15	61%	4.68
	subsurface (4)	3–67	25 ± 15	20 ± 10	36 ± 27	2.21 ± 0.59	35 ± 16%	
52	surface (new)	0–3	42	24	66	2.84	64%	2.98
	subsurface (5)	3–65	22 ± 9	18 ± 6	28 ± 13	2.02 ± 0.40	33 ± 14%	
53	surface (new)	0–4	11	8	16	2.41	47%	3.04
	subsurface (4)	4–36	19 ± 15	16 ± 10	25 ± 21	1.87 ± 0.32	28 ± 11%	
54	surface (new)	0–4	20	13	35	3.33	65%	5.06
	subsurface (3)	4–32	21 ± 17	18 ± 13	28 ± 24	2.08 ± 0.25	31 ± 7%	
55	surface (new)	0–3	17	11	25	2.54	54%	2.78
	subsurface (4)	3–32	21 ± 8	20 ± 8	23 ± 8	1.58 ± 0.24	17 ± 9%	
56	surface (new)	0–5	14	11	19	2.36	45%	3.23
	subsurface (4)	5–65	8 ± 3	7 ± 3	10 ± 4	2.00 ± 0.06	32 ± 2%	
57	surface (new)	0–6	15	13	19	2.10	35%	3.27
	subsurface (4)	6–30	12 ± 7	11 ± 6	15 ± 10	1.86 ± 0.22	26 ± 7%	
58	surface (new)	0–6	18	15	24	2.21	37%	3.74
	subsurface (5)	6–50	17 ± 15	19 ± 9	24 ± 25	2.02 ± 0.44	32 ± 15%	
59	surface (new)	0–4	63	25	105	3.11	76%	3.04
	subsurface (3)	4–30	30 ± 15	22 ± 8	42 ± 24	2.21 ± 0.25	40 ± 9%	
60	surface (new)	0–10	10	8	13	2.37	43%	3.60
	subsurface (5)	10–45	30 ± 5	25 ± 4	39 ± 8	2.10 ± 0.13	34 ± 5%	
61	surface (new)	0–10	12	7	19	2.83	62%	3.43
	subsurface (5)	10–50	23 ± 9	20 ± 7	28 ± 13	1.87 ± 0.26	26 ± 9%	
62	surface (new)	0–4	44	39	55	1.97	29%	4.50
	subsurface (5)	4–28	13 ± 6	12 ± 6	14 ± 6	1.51 ± 0.10	15 ± 3%	
63	surface (new)	0–4	27	22	35	2.18	37%	3.73
	subsurface (3)	4–28	13 ± 5	12 ± 5	14 ± 5	1.64 ± 0.09	19 ± 3%	
64	surface (new)	0–5	26	21	34	2.22	38%	3.76
	subsurface (4)	5–35	30 ± 23	26 ± 19	37 ± 30	1.79 ± 0.11	24 ± 3%	
65	surface (new)	0–3	51	36	73	2.52	51%	3.34
	subsurface (5)	3–32	24 ± 9	20 ± 8	31 ± 11	2.14 ± 0.11	36 ± 4%	
66	surface (new)	0–10	31	28	38	1.92	27%	{3.73}
	subsurface (5)	10–46	43 ± 16	37 ± 12	55 ± 22	2.03 ± 0.18	31 ± 6%	
67	all new snow	drift	6	6	8	2.13	35%	{3.73}
			17	15	21	1.95	29%	
			30	24	42	2.36	43%	

winter, but for most of the Canadian sites (excepting sites 66 and 67), snow cover is more continuous, with snow depth generally increasing through the winter and early spring.

As discussed above, pairs of samples were collected in parallel at each site, in glass jars, and food-grade bags. These paired samples enable us to identify any systematic difference in the samples collected in the plastic bags versus the glass jars. For our 250 sample pairs, the average difference (bag-jar) in C_{BC}^{max} was 5 ± 43% and in $\mathring{A}_{tot}$ was 0.09 ± 0.20. Consistent with our precampaign tests, the food-grade bags do not appear to scavenge a significant fraction of the sampled particles; in fact, concentrations were, on average, higher for the bags by 5%, though not significantly so given the variability in side-by-side pairs. Because there is no systematic difference in samples collected in bags versus in jars, the results we report here from the ISSW analysis for each sample layer are averages of the results from bag/jar pairs in each sample layer.

The paired samples also allow us to measure variations in particulate absorption at small (~1 m) spatial scales. This is measured by calculating the absolute value of the difference in side-by-side sample pairs. The absolute difference was, on average, 32% ± 28% for C_{BC}^{max} and 0.16 ± 0.15 for $\mathring{A}_{tot}$. The average value of $\mathring{A}_{tot}$ across the whole campaign was 2.23 (range: 1.2–4.4), so this corresponds to difference of about 7% in $\mathring{A}_{tot}$ for paired samples. Thus, as is to be expected, particle concentration varies relatively more than does particle type at this small spatial scale. A small-scale concentration variation of ~30% was also found in paired samples

©2014. American Geophysical Union. All Rights Reserved.

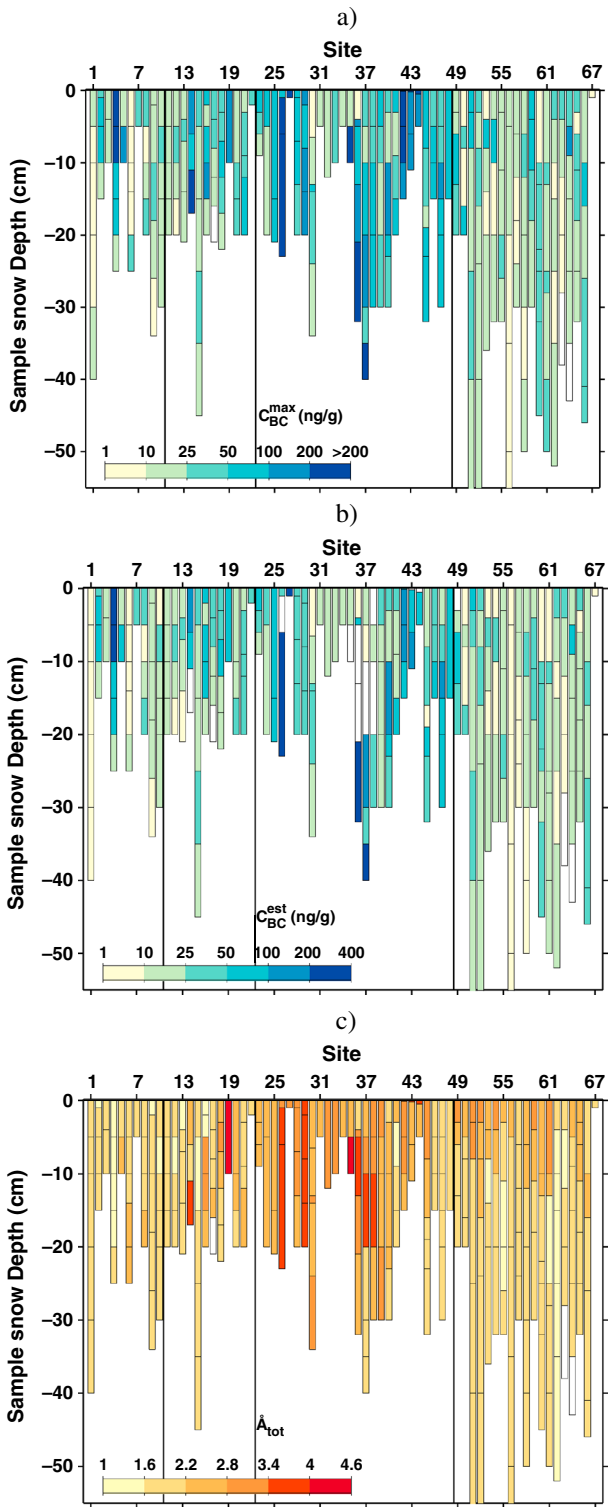

Figure 7. Vertical profiles of (a) C_{BC}^{max}, (b) C_{BC}^{est}, and (c) $Å_{tot}$ at each sampling site. Each of Sites 22, 48, and 67 actually comprise several nearby snow pits (a few kilometers apart) for studies of local variability. The values shown here are the average of all subsites at each of these sites. White bars indicate unsampled layers (as shown also in Figure 6) or where we could not estimate the snow BC mixing ratio. Vertical black lines demarcate the four sampling regions (Figure 1).

from the Arctic [*Doherty et al.*, 2013]. Note that some of this variation may be due to vertical variations being aliased into horizontal variation if pairs of samples were not gathered from identical snow layers, since perfect alignment of side-by-side samples is not possible. Indeed, the average absolute difference in column-integrated C_{BC}^{max} for side-by-side profiles was 23%, somewhat lower than the difference in C_{BC}^{max} sample pairs at a given depth.

Regional medians and standard deviations of C_{BC}^{equiv}, C_{BC}^{max}, C_{BC}^{est}, f_{NBC}^{est}, and $Å_{tot}$ are shown in Table 1, and site-specific values given for each of the four regions in Tables 2–5. C_{BC}^{equiv}, C_{BC}^{est}, and $Å_{tot}$ are shown as a function of sample depth in Figures 7a–7c, and C_{BC}^{est}, and $Å_{tot}$ (for surface snow samples only) on a map in Figures 8a and 8b. In addition, in Figure 8c we show the equivalent BC mixing ratio that would be needed to account for the 300–750 nm absorption by all non-BC constituents, calculated as $C_{BC}^{equiv} \times f_{NBC}^{est}$. Figures 8a and 8c can thus be compared for the relative roles of BC and non-BC components in snow albedo reduction at each site.

In the PMF analysis the best fit was achieved with five factors/sources. However, two of these sources, associated with metal smelting or refining, together accounted for only ~6% of the light absorption. The remaining 94% of C_{BC}^{max} is associated with factors identified as soil, biomass burning, and pollution (Figure S3). The interpretation of the soil factor as soil is based on the high loadings for Al, K, Ti, V, Ca, and As, all well-known soil constituents. The biomass burning attribution is based primarily on the high loading of levoglucosan, a unique marker for wood combustion, but also on high levels of carboxylic acids and mannitol. The pollution factor attribution is based on the high loadings of sulfate, oxalate, and nitrate, again well-known markers for pollution emissions. The biomass burning factor may include both open-burning (e.g., wildfire) sources and biofuel (e.g., wood burning in stoves/heaters), as the two are chemically indistinguishable in this data set. The pollution factor includes chemical

©2014. American Geophysical Union. All Rights Reserved.

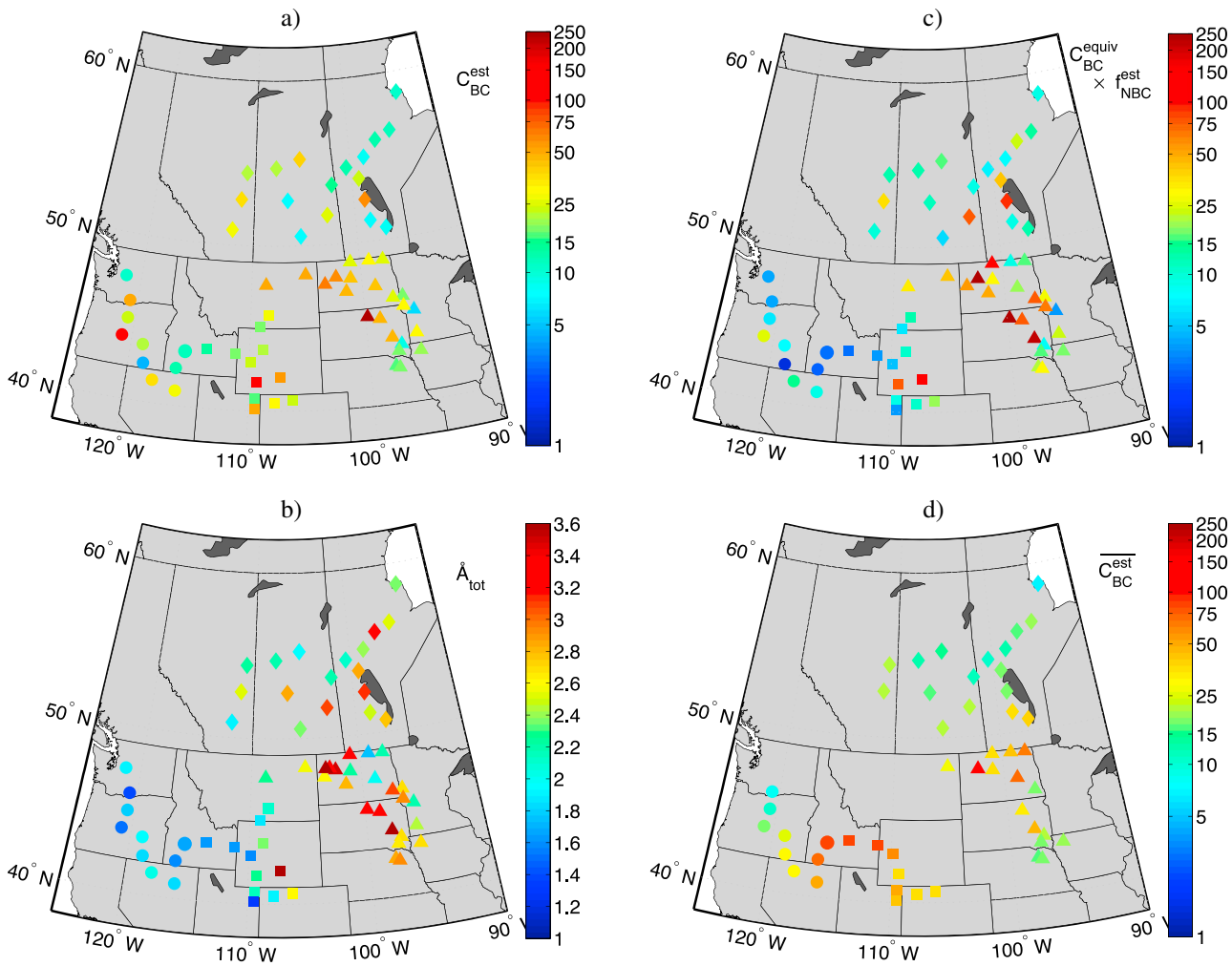

Figure 8. (a) C_{BC}^{est} and (b) $\mathring{A}_{tot}$ for the surface layer at each site, with symbols by region (see Figure 1). Many of these samples are of new snow (Figure 6 and Table 2). (c) Estimated BC-equivalent mixing ratio (ng g^{-1}) needed to account for spectrally integrated (300–750 nm) absorption of sunlight by non-BC components in snow. (d) Estimated average snow BC mixing ratio, $\overline{C_{BC}^{est}}$, calculated by integrating snow water content and BC mass over the entire snowpack (see Table 3).

tracers associated with fossil fuel combustion and chemical processing. However, we expect light-absorbing particles from these sources to be associated predominantly with fossil fuel combustion, so this can effectively be considered a fossil fuel factor.

The soil factor is somewhat difficult to interpret. Soil itself is a receptor for dry deposition (or even wet deposition followed by snow melt—which does happen in this region) from other sources. Saltation and redeposition of soil onto the surrounding snow areas is likely to result, at least to some extent, not only in deposition of light-absorbing particles intrinsic to the soil itself (e.g., HUmis-LIke Substances, or HULIS) but also of particles whose primary source was biomass burning or pollution.

Keeping this possible complexity in mind, the fraction of absorption (as measured using C_{BC}^{max}) due to the soil, biomass burning, and pollution/fossil-fuel factors (F_{SOIL}, F_{BB}, and F_{FF}) from the PMF analysis are given in Table S2. The PMF analysis allows some factors to contribute negative fractions to absorption (e.g., see Figure 3), which is of course unphysical. To display the data (Figure 9), we have set all negative fractions F_{SOIL}, F_{BB}, and F_{FF} to zero and scaled the remaining fractions so that they sum to 1.0, yielding adjusted values F'_{SOIL}, F'_{BB}, and F'_{FF}.

In addition to calculating snow BC mixing ratios in sample layers, a useful metric for comparison to models is the mass of BC deposited over a specified period of time, ideally a month or season in order to average

©2014. American Geophysical Union. All Rights Reserved.

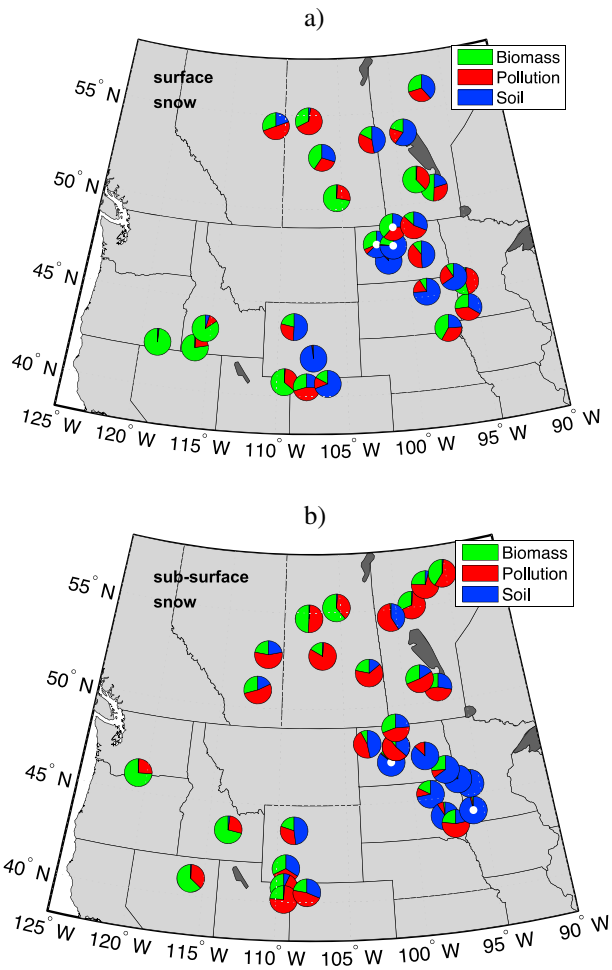

Figure 9. Fractional contributions to 650–700 nm particulate absorption (as measured by C_{BC}^{max}) by soil (F'_{SOIL}), biomass (F'_{BB}) combustion, and pollution (F'_{FF}) from the PMF analysis for (a) surface snow and (b) subsurface snow samples. Pie charts with white dots in the middle indicate sites where "synthetic" OC_{abs} values were used in the PMF analysis (see section 3.3).

across many wet deposition events. Since our sample profiles are essentially snapshots in time, we do not know over what period the measured snow accumulated, whether snow cover at the sample site had been intermittent, or how much snow water (and BC) were lost to melting and sublimation during the snowpack's lifetime. Nonetheless, at sites with continuous snow cover and little expected melting, such as our Canadian sites, total column BC mass (ng cm^{-2}) can be considered a lower bound on the total BC mass deposited during the snow accumulation season, up to our sampling date. At other sites, measured snow water equivalent (SWE; g cm^{-2}) at the time of sampling together with time histories of SWE from, e.g., Moderate Resolution Imaging Spectroradiometer (http://nsidc.org/data/myd10cm; http://nsidc.org/data/myd10cm) and/or SNOw Data Assimilation System (SNODAS) data (http://nsidc.org/data/g02158) could be used to estimate the deposition period of the observed snowpack. In addition, the average BC mixing ratio in the snow column $\left(\overline{C_{BC}^{est}}\right)$ (Table 6 and Figure 8d) may be a better metric for model comparisons than the surface sample's C_{BC}^{est}. Here we calculate $\overline{C_{BC}^{est}}$ (units: ng g^{-1}) as the sum of all BC in the snow column divided by the total snowpack SWE. By integrating across the entire snowpack, $\overline{C_{BC}^{est}}$ averages the effects of, e.g., heavy and lighter snowfall events and variations in BC mass deposition rates. It also smooths out the effects of in-snow processes, such as melting/percolation/refreezing, that redistribute the BC within the snow column but that do not change the total mass of BC present. Indeed, $\overline{C_{BC}^{est}}$ is more regionally consistent (Figure 8d) than is C_{BC}^{est} in the surface layer (Figure 8a).

C_{BC}^{max}, C_{BC}^{est}, and $\mathring{A}_{tot}$ vary regionally (Tables 1 and 2 and Figures 7, 8a, and 8b), as does the relative importance of BC and non-BC components (Figure 8c). However, variations within a given region are sometimes comparable to or greater than variations between the regions, so below we discuss the results within each subregion.

3.1. Pacific Northwest (Sites 1–10)

Snow samples in the Pacific Northwest region (Figure 1) were mostly collected from grass/shrublands or open areas at higher elevations (Figure 2a and Table S1) and include two sites (7 and 8) in northern Nevada. In this region, the snow was not very deep but was usually evenly distributed around our sampling area. $\mathring{A}_{tot}$ was generally less than 2.0 (Tables 1 and 2 and Figures 7 and 8), so that most of the snow particulate absorption is due to BC (f_{NBC}^{est} ~10–30%). The PMF analysis yielded results for only a few of the surface and subsurface samples each in this region, but these sites consistently have biomass burning as the dominant source of particulate light absorption, with pollution accounting for essentially all of the remaining absorption (Figure 9).

©2014. American Geophysical Union. All Rights Reserved.

Table 6. Total Snow Water Equivalent (SWE) and Estimate of Total Snowpack BC Mass in a 1 cm^2 Column of Snow, for Sites Where the Snow Profile Sampled Was Considered Representative of the Local Region[a]

Site #	Date Sampled (2013)	Integrated SWE (g cm^{-2})	Integrated BC (ng cm^{-2})	Snowpack Average BC Mixing Ratio (ng g^{-1})
1	10 Jan	11.1	75	7
2	28 Jan	4.6	148	32
3[a]	29 Jan	2.4	62	26
4	29 Jan	5.3	489	93
5	30 Jan	3.6	218	61
6	31 Jan	8.1	69	8
8	1 Feb	6.7	117	17
9	1 Feb	10.6	133	13
10	3 Feb	9.3	141	15
11	3 Feb	4.3	54	13
12[b]	4 Feb	3.4	53	16
13	4 Feb	4.7	83	18
14	5 Feb	4.6	399	87
15	5 Feb	10.4	240	23
16	7 Feb	4.4	198	45
17	8 Feb	6.5	129	20
18	9 Feb	6.7	179	26
24	17 Feb	6.0	168	28
28[c]	19 Feb	6.0	201	33
29	19 Feb	6.7	315	47
30	22 Feb	6.8	147	22
31[b]	22 Feb	0.2	4	18
32[b]	22 Feb	2.3	37	16
33[b]	22 Feb	1.2	22	18
34[b]	23 Feb	0.9	16	19
39	27 Feb	9.2	169	18
40	28 Feb	8.4	610	73
41	28 Feb	5.3	192	36
42	1 Mar	4.6	504	110
45	2 Mar	8.5	297	35
46[c]	2 Mar	4.1	168	41
47	3 Mar	7.6	505	67
49[c]	6 Mar	5.0	198	39
50	7 Mar	5.0	181	36
51[c]	7 Mar	17.1	304	18
52	8 Mar	13.9	243	18
53[c]	8 Mar	8.1	105	13
54[c]	11 Mar	6.4	101	16
55[c]	11 Mar	8.9	168	19
56	12 Mar	33.6	243	7
57[c]	13 Mar	6.6	71	11
58	14 Mar	11.1	131	12
59	14 Mar	7.8	163	21
60	15 Mar	13.7	298	22
61	18 Mar	14.1	219	16
62	19 Mar	11.5	173	15
63[c]	19 Mar	6.9	88	13
64	20 Mar	8.4	174	21
65	20 Mar	7.6	164	22

[a]The integrated BC is calculated from the SWE and C_{BC}^{est} in each sample layer. The snowpack average BC mixing ratio, C_{BC}^{est}, is also given. At Sites 17, 18, and 56, we did not sample the entire snow depth. Here the values were calculated by extrapolating SWE and C_{BC}^{est} to the bottom of the snowpack, assuming the snow density and C_{BC}^{est} were the same for the unsampled snow as that in the bottommost snowpack layer.

[b]Snowpack was of all new snow on bare ground; i.e., snow cover at this site is intermittent.

[c]Site was on frozen lake/river/swamp ice, so snowpack only includes snow/BC that fell after the surface froze.

©2014. American Geophysical Union. All Rights Reserved.

There also appears to be some seasonal dependence to sources, with F'_{BB}:F'_{FF} higher for the surface samples (middle winter) than for the subsurface samples (early winter) (Figure 9).

Site 4, situated in central Oregon, had the highest C_{BC}^{max} concentration in the Pacific Northwest region and also the highest fraction of light absorption due to non-BC constituents (64%) in the entire data set, the latter in accord with the brown coloration of the sample filter for this site. Additionally, sulfate concentrations exceeded 3000 ppbm (true of only seven of the samples across the entire data set), and the levoglucosan concentration was well above the data set mean (10.3 ppbm compared to a mean of 8.0 ppbm). The site was located ~50 km southeast of Bend, Oregon (metropolitan population of ~170,000), and we surmise that the high species concentrations, e.g., formate, sulfate, levoglucosan, Ni, Zn, Pb, Cr, and mannitol, reflect anthropogenic emissions such as wood stove smoke and diesel and gasoline combustion exhaust.

In contrast, the cleanest site of the entire campaign was site 6, in southeast Oregon, with surface snow $C_{BC}^{max} = 5$ ng g^{-1} and $C_{BC}^{est} = 4$ ng g^{-1}. This is comparable to concentrations in the cold snow of the high Greenland plateau [e.g., *Hagler et al*., 2007a, 2007b; *McConnell et al*., 2007; *Doherty et al*., 2010]. Most sites in the Pacific Northwest had snow BC mixing ratios of ~5–40 ng g^{-1} (Table 2) but some were dirtier (Table 2 and Figures 7 and 8), possibly in part due to the fact that snow at some of these sites was melting (Figure 6). *Clarke and Noone* [1985] sampled snow at three sites on the Washington State Olympic Peninsula in late March 1984. Using a similar method to ours, they estimated snow BC mixing ratios of 10, 15, and 19 ng g^{-1} at the three sites, similar to the concentrations we found farther east and south in the Pacific Northwest.

3.2. Intramountain Northwest (Sites 11–22)

Sites 11–22 are located in the Intramountain Northwest, transitioning from the dry foothills of south-central Idaho (sites 11–12); east into west-central Wyoming (site 13); through southern Wyoming, the northeast corner of Utah, and the northern edge of Colorado, where there are both lower elevation, drier sites (14, 16, and 19) and sites higher in the mountains (15, 17, and 18). We then moved north, following the east edge of the Rockies foothills into the plains of Montana (sites 20–22). The terrain for these sites was more variable than in the other three regions. Sites in wetter areas closer to high mountains generally have particles with lower $\mathring{A}_{tot}$ and a higher fraction of absorption due to biomass and/or fossil fuel burning than due to soil. Sites in dry, broad basins (e.g., 14, 16, and, in particular, 19; Figure S2) have higher $\mathring{A}_{tot}$, consistent with a larger fraction of the absorption being due to local soil. The soil from sites 19 and 20 was notably redder ($\mathring{A}_{soil} > 6$) than at all other sampling sites (Figures 4 and 5), so even small contributions of this soil to total particulate light absorption have a significant effect on the color of snow particles ($\mathring{A}_{tot}$). Snow BC mixing ratios were marginally higher here than in the Pacific Northwest with C_{BC}^{est} typically ~10–50 ng g^{-1} (Table 3). An exception is site 14, where C_{BC}^{est} of newly fallen snow was 147 ng g^{-1}. Sulfate at this site was also exceptionally high (>3000 ppbm). Site 14 is 30 km east of the Green River coal-fired power plant (30 MW) and ~90 km due east of the Naugton plant (707 MW; 20,664 tons of sulfur dioxide emitted per year). Combustion aerosol and fugitive coal dust from these plants may be contributing to the observed high sulfate and BC mixing ratios in snow. The site is also ~20 km from highway I-80 and so may be influenced by diesel truck traffic.

A transection of newly fallen snow samples at six sites approximately 5, 10, 15, 20, 25, and 40 km east/south-east of Billings, Montana (site 22) showed a moderate decline in C_{BC}^{est} with distance from the city, from $C_{BC}^{est} = 39$ ng g^{-1} to 24 ng g^{-1}. The fraction of non-BC absorption was nearly unchanged moving away from the city ($f_{NBC}^{est} = 34\%$ to 28%). While no chemical/PMF analysis was conducted for these samples, these values of f_{NBC}^{est} are consistent with those of other sites where biomass and/or fossil fuel combustion are the primary sources of snow particulate light absorption.

3.3. Northern U.S. Plains

In the Northern U.S. Plains region, there is a strong gradient in snow depth from south-west to north-east (Figure S2), with sites 24–33 essentially following the snow line. During our sampling of this region (mid-February), there was almost no snow in eastern Montana, and none in southwest North Dakota and western South Dakota (Figure S2). At site 23 in Montana, we collected melting snow on the north side of a hill, because the rest of the area was snow free (Figure 2c). Surface samples were of newly fallen snow at most of sites 26–36, and there were moderate to significant winds accompanying this snowfall at almost all of these sites. At sites farther north and east, the snow was generally deeper, but much of this snow was also wind packed (Figure 6).

©2014. American Geophysical Union. All Rights Reserved.

At sites 26 and 27 in the Dakotas, the snow was shallow and there were very strong surface winds (30+ knots, or 15+ m s). Here we collected drift snow downwind of several trees (Figure 2d). At site 26, newly fallen drifted snow and two layers in old drift snow were sampled. The drift snow at sites 26 and 27 was quite dirty (C_{BC}^{max} ~520–620 ng g^{-1}) compared to the new snow at site 26 (C_{BC}^{max} = 60 ng g^{-1}). A significant fraction of the total particulate absorption in the drift snow was attributed to BC, so C_{BC}^{est} is also notably high in these layers: ~300 ng g^{-1}. This could be due to large amounts of soil being mixed in to the drift snow, and light absorption from that soil being erroneously attributed to BC, or it could be that these sites were close enough to combustion sources that they were exposed to episodically high BC deposition.

Significant vertical variations in C_{BC}^{max} were also observed at sites 36 and 37. Site 36 included a new snow sample that was very clean (C_{BC}^{max} = 7 ng g^{-1}; C_{BC}^{est} = 6 ng g^{-1}), then three layers with C_{BC}^{max} ~135–175 ng g^{-1} (5–21 cm depth), then a single very dirty layer (C_{BC}^{max} 480 ng g^{-1}; 21–32 cm depth). In all but the bottommost of these layers, almost all absorption was attributed to non-BC absorbers. Non-BC absorption for the dirtiest, bottommost layer was low (f_{NBC}^{est} = 37%), so C_{BC}^{est} is 420 ng g^{-1}. At site 37, the top three layers of the snowpack (0–20 cm) was cleaner than the bottom three layers (20–40 cm), with C_{BC}^{max} in the six layers 31, 27, 85, 181, 50, and 434 ng g^{-1}, respectively. In the top three layers, almost all of the absorption was attributed to non-BC components, but in the bottom three layers, f_{NBC}^{est} was only 20–30% ($\mathring{A}_{tot}$ 1.7–2.1) leading to estimated BC mixing ratios (C_{BC}^{est}) of 240, 63, and 525 ng g^{-1}, respectively, moving down in the snowpack.

In general, total particulate light absorption in the Northern Great Plains region is higher than in the other sample regions, as are $\mathring{A}_{tot}$ and f_{NBC}^{est} (Tables 1 and 2 and Figures 7 and 8). Consistent with this, the PMF analysis attributes a large fraction of 650–700 nm absorption to soil—for the sites in the Dakotas and Minnesota in particular (Figure 9). Snow BC mixing ratios were higher in the northern and western sites in this region, with notably lower BC mixing ratios in surface samples from sites 30 to 37. Most of these samples were of newly fallen snow that fell over a period of a few days in what local meteorologists dubbed "Winter Storm Q."

Of the nonsoil particulate absorption, pollution appears to play a stronger role in this region than in the Pacific Northwest or Intramountain Northwest—i.e., F'_{FF}:F'_{BB} is higher (Figure 9). We again caution that for f_{NBC}^{est} >50% (as is the case for many of the samples in this region), the ISSW may be overestimating BC mixing ratios by a factor of 1.5–2 or more [*Schwarz et al.*, 2012]. For these samples, soil is likely playing an even more dominant role—and BC a smaller role—in snowpack albedo reduction than is indicated by our data.

Samples of newly falling snow were gathered in Grand Forks, North Dakota, and at two adjacent sites ~20 km downwind of the city (site 48). The snow BC mixing ratio 20 km outside the city was about one third to one half that in the city. As in the transect away from Billings, MT, the fraction of non-BC absorption was lower outside the city (f_{NBC}^{est} = 26% and 29%) than in the city (f_{NBC}^{est} = 33%), though again not significantly so. Also, as near Billings, there is no chemical/PMF analysis for these sites, but their f_{NBC}^{est} is similar to that for sites with a fossil or biomass combustion source of snow particles.

The sites around Williston, North Dakota, are of special interest because of the recent very rapid growth in oil exploration/extraction in the Baaken Oil Fields. Site 25 is immediately south, and sites 42–44 are directly east of Williston and are in the heart of oil-drilling activity. We expected that the snow in this region might have high BC mixing ratios because of the combination of gas-flaring and diesel truck traffic. But in addition, traffic on dirt roads has dramatically increased. In the field, it was visually apparent that the combination of low snow cover, high winds, heavy road use, and soil disturbance near roads, oil rig sites, and areas cleared for housing was exposing a lot of dirt, which could readily be lofted and deposited to snow. C_{BC}^{max} and C_{BC}^{est} are not particularly elevated at site 25, but sites 42–44 were very dirty: C_{BC}^{max} for the surface layers at these sites is 356, 884, and 598 ng g^{-1} and is ~150–250 ng g^{-1} for the subsurface layers. $\mathring{A}_{tot}$ is also quite high for the surface layer samples (3.5–3.9) but is more moderate for the subsurface layer (~2.7). Because $\mathring{A}_{tot}$ is so high in the surface layer samples, almost all absorption is attributed to non-BC components (i.e., f_{NBC}^{est} 80–100%), so the snow BC mixing ratio is not estimated. For the subsurface layers, f_{NBC}^{est} is about 50% and C_{BC}^{est} is about 70–110 ng g^{-1}. In comparison, C_{BC}^{est} at sites 40–41 and 45–47 was usually ~20–60 ng g^{-1}.

Five sites in the Dakotas (26, 27, 42, 43, and 44) had exceptionally high sulfate concentrations (>3000 ppmb). These sites are oriented in a line running northwest to southeast and roughly along the Missouri River valley. This line is also approximately coincident with a string of six coal-fired power plants commencing near

©2014. American Geophysical Union. All Rights Reserved.

Bismarck, ND, and running along the Missouri river to the NW. Collectively, these plants emit in excess of 125,000 tons of sulfur dioxide per years as well as many tons of fly ash. While it is thus tempting to attribute snow sulfate and any associated high C_{BC}^{max} concentrations to this source, the chemical data as a whole suggest a more complex scenario. For example, five of the seven highest values of noncrustal vanadium occur in samples from this region. Noncrustal vanadium is a well-known tracer for petroleum combustion and refining, particularly for crude oil [cf., *Yan et al*., 2012; *Leck et al*., 2002]. Furthermore, the field gas flaring used in oil extraction operations is a substantial source not only of BC and gaseous sulfur such as sulfur dioxide [cf., *Environmental Protection Agency*, 2000; *Pikelnaya et al*., 2013] but also of vanadium [*Ite and Ibok*, 2013]. This should be particularly true for the extraction from the Bakken formation since the black shale of this formation has the highest concentrations of vanadium of any crustal mineral ensemble. On the other hand, concentrations of Al, an excellent and well-known tracer of soil/mineral dust, are also relatively high in this region, and of course, soil and dust are also well-established sources of light-absorbing aerosol [e.g., *Zhang et al*., 2013]. The sources of C_{BC}^{max} for this region are thus potentially multiple and unlikely to be resolved by single correlation or linear modeling.

The optimized PMF did not include results for most samples from sites 25 and 42–44. Some of the samples were excluded because OC_{abs} values were not available from the *Dang and Hegg* [2014] analysis. OC_{abs} is highly correlated with $\mathring{A}_{tot}$ (not shown), so for a set of five samples from these four sites we generated synthetic OC_{abs} values based on $\mathring{A}_{tot}$. The quantitative relationship between $\mathring{A}_{tot}$ and OC_{abs} was estimated by linearly regressing $\mathring{A}_{tot}$ onto OC_{abs}. The regression utilized 51 data points (some points were eliminated due to marginal signal to noise ratios) and had an r^2 value of 0.6 with a p of 0.01. We then reran the PMF, including these synthetic samples (see Table S2). This reduced Q by only a few percent and did not significantly change the factor fingerprints or the relative contributions of each factor to absorption. The factor contributions from this second PMF run for these five samples only are included in Figure 9 and are flagged by white dots in the center of the pie chart; all other results given are from the main PMF run.

Consistent with the high values of $\mathring{A}_{tot}$, soil dominates snow particulate light absorption in this region (Figure 9). This is particularly true for the subsurface samples, which correspond to a deposition period when snow depth—and possibly also snow cover—was less. The remaining absorption is generally due more to pollution than to biomass combustion, though at sites 42 and 45 F'_{BB}:F'_{FF} is >1, which is surprising given the proximity to the Bakken oil field activities. As in our other sample regions, biomass combustion plays a relatively stronger role in total particulate light absorption in the surface samples (Figure 9a) than in the subsurface samples (Figure 9b), indicating a shift in sources as the winter progresses.

3.4. Canada

The transition from North Dakota into Canada was also a transition to a deeper snowpack (Figure S2), and all surface samples in Canada were of new snow. At the northernmost site 56, near Churchill on the coast of Hudson Bay, snowpack depth varied dramatically. There was bare ice exposed in some locations but >1 m of snow in the drift where we sampled. At this site, we sampled only the top 65 cm of the snowpack.

One of the chemically analyzed samples from site 50, situated on a frozen lake surface in rural Manitoba, appears anomalous. The formate and sulfate concentrations in the "subsurface" sample (collected at 18 cm depth) were over 12,000 and 20,000 ppbm, respectively. These were, by far, the highest concentrations for these species in the entire data set. These are not credible for a rural site, indeed scarcely so for an urban site. While the origin of the apparent contamination is not clear, we consider the sample compromised and do not include it in the PMF modeling.

The snow in Canada was generally cleaner than in the other three regions. $\mathring{A}_{tot}$ also tended to be lower than in the Intramountain and Great Plains regions, and it was lower deeper in the snowpack than near the surface (Figure 7). Consistent with the optical data, the PMF analysis shows a smaller contribution by soil to light absorption at the Canadian sites than in the Intramountain and Northern U.S. Plains regions. It also shows a greater contribution by soil to C_{BC}^{max} for the Canadian surface samples than in the Canadian subsurface samples (Figure 9a versus 9b). The ratio F_{FF}:F_{BB} also appears to be lower in the surface samples than in the subsurface samples (Figure 9a versus 9b), again indicating a shift in the dominance of fossil versus biomass combustion sources with season.

©2014. American Geophysical Union. All Rights Reserved.

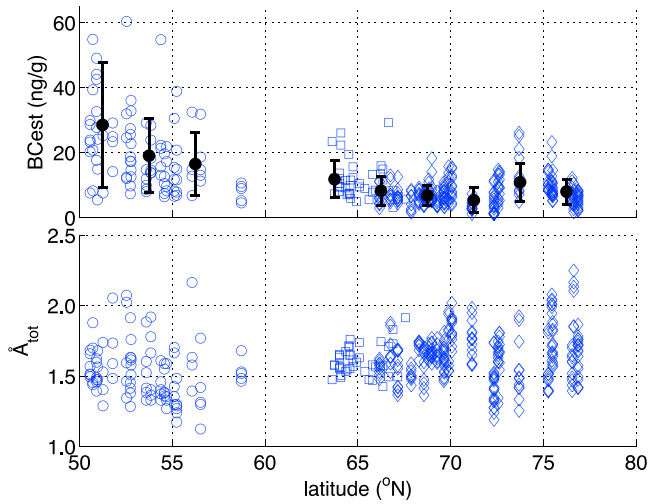

Figure 10. (top) C_{BC}^{est} and (bottom) $\mathring{A}_{tot}$ as a function of latitude, for all sample layers at the Canadian sites (49–67) from the 2013 field campaign (circles), and from samples in sub-Arctic Canada in 2007 (squares) and Arctic Canada in 2009 (diamonds). The latter two data sets were presented by *Doherty et al.* [2010]. The average and standard deviation of C_{BC}^{est} within 2.5° latitude bands are also shown (Figure 10 (top); error bars).

Three samples of new snow collected as we approached the city of Calgary from the east show BC mixing ratios increasing toward the city, with C_{BC}^{est} 6 ng g^{-1}, 15 ng g^{-1}, and 24 ng g^{-1} at 60 km, 45 km, and 30 km from the Calgary city limits. Contributions to absorption by non-BC components were higher and more variable (35%, 29%, and 43%) than for the new snow samples collected along the transect out of Billings, MT (site 22) or the new snow collected in and 20 km East/Southeast of Grand Forks, ND (site 48). This may be because the snow at the Calgary sites (67) was thinner, all three sites were on farmland, and it was quite windy.

3.5. Latitudinal Gradients: Great Plains to Canadian Boreal Forest

In previous field campaigns, samples were gathered in an east-west traverse across sub-Arctic Canada (~63°N–67°N) in 2007, and in the Canadian Arctic (67°N–77°N) in 2009. Both of these campaigns included sites directly north of our 2013 sample region (Figure S4). The 2007 and 2009 samples were also analyzed with the ISSW spectrophotometer [*Doherty et al.*, 2010] and chemical and PMF analyses used to determine sources of light absorption [*Hegg et al.*, 2009, 2010]. In Figure 10, we have combined these two data sets with our current Canadian data set and plotted C_{BC}^{est} and $\mathring{A}_{tot}$ for all samples as a function of latitude. (Note that in Figure 10 the 2007 and 2009 values of C_{BC}^{est} from *Doherty et al.* [2010] were scaled down by a factor of 1.12 to account for a change in the 650–770 nm mass absorption coefficient of 5.0 m^2 g^{-1} for our old calibration standards to 5.6 m^2 g^{-1} for the fullerene standards used here.)

Estimated BC mixing ratios average ~30 ng g^{-1} in southern Canada, then generally decrease with latitude up to the northernmost 2013 sampling site (57.8°N), where they are about 10 ng g^{-1} (Figure 10). The 2007 and 2009 data set spans 64–77°N, and within this latitude band C_{BC}^{est} shows no apparent latitudinal trend, typically varying between 5 and 15 ng g^{-1}. Variability in C_{BC}^{est} within latitude bands also decreases, from ~65% at lower latitudes to ~50% at higher latitudes, consistent with higher latitudes being further from sources. Since the data in Figure 10 include samples from all snow depths, this variability accounts for both spatial variations and seasonal variations.

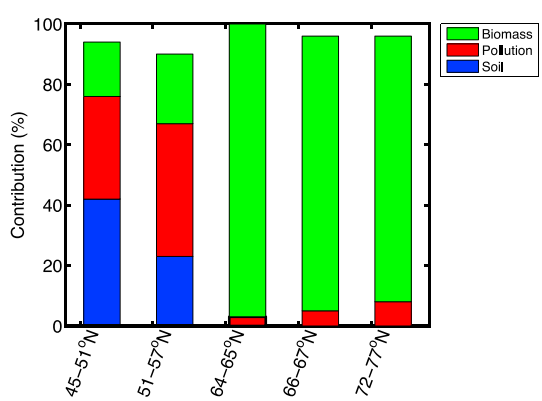

Figure 11. Attribution of snow particulate 650–700 nm absorption (C_{BC}^{max}) to soil, biomass, and pollution, for samples within latitude bands in Canada, from PMF analyses. Metal smelting sources (not shown) also contribute a small fraction of absorption in some latitude bands. As in Figure 11, this combines analyses of the 2013 field sample (up to 60°N), and samples gathered in previous field campaigns in 2007 and 2009, presented originally by *Hegg et al.* [2009, 2010]. See Figure S4 for location of sites included in each latitude band.

Although $\mathring{A}_{tot}$ shows no trend, latitudinal gradients in sources can be seen in the PMF factor contributions to C_{BC}^{max}, shown in Figure 11 for latitude

©2014. American Geophysical Union. All Rights Reserved.

bins spanning our sites in northern South Dakota/western Minnesota to those containing the northernmost sites in the 2009 Arctic Canada survey of *Doherty et al.* [2010] and *Hegg et al.* [2010] (Figure S4). The 45°N–51°N bin encompasses the Northern U.S. Plains sites, plus Canadian sites 49 and 60. Most of the absorption in this band is attributed to soil and pollution, with a smaller contribution by biomass combustion. The 51°N–57°N band includes all other 2013 Canadian sites—with the exception of site 56, which lacks chemical data (and therefore a PMF solution). The soil contribution to absorption is less here than in the Plains; F_{FF} is still substantial, and F_{FF}:F_{BB} about the same as in the Plains. The 64°N–65°N band includes sites from the 2007 survey; the 66°N–67°N band sites from 2007 and 2009; and the 72°N–77°N band sites from 2009. For the 2007 and 2009 data sets, the PMF solution did not include a soil factor, with pollution and biomass combustion accounting for essentially all snow particulate absorption. In all of these northern bands, F_{BB} dominates absorption. This decrease in the role of soil with latitude is consistent with a northward increase in snow depth [*Potter*, 1965], and with the fact that soil in the southern Canadian and U.S. Great Plains is disturbed by agricultural activity, whereas in the Canadian Arctic the soil is less disturbed. It also may be influenced by the fact that most of the 2009 sampling sites were located on lakes, sea ice, or ice caps remote from soil sources.

To investigate the change in F_{FF}:F_{BB} with latitude shown in Figure 11, we conducted a back trajectory cluster analysis. Ideally we would run back trajectories for the times when absorbing particles were deposited to snow. Since we do not know when deposition occurred, we ran the NOAA HYbrid Single-Particle Lagrangian Integrated Trajectory (HYSPLIT) model, version 4 [*Draxler and Rolph*, 2012] (http://ready.arl.noaa.gov/HYSPLIT.php) 4 times a day starting 30 days before the site sample profile was collected, up to the collection day. The resulting trajectories were then grouped into five clusters. A representative set of these analyses are shown in Figure S5. Air masses almost always originated from the north to north-west of the sample site, with a more west/north-west origin at the southernmost sites and a more northern origin at the northernmost sites. At the southernmost sites, air masses tended to pass over western Canada, with very little contribution from Alaska and Siberia (e.g., 2013 sampling sites 28 and 45; Figures S4, S5a, and S5b). Air reaching the sites farther north increasingly pick up contributions from Alaska and Siberia. The latter in particular is known to be a significant source of biomass combustion, with biomass burning occurring earlier in the spring than at other northern high latitudes [*Lavoué et al.*, 2000]. These air mass transport pathways imply very little contribution of sources within our study region to the Arctic.

4. Discussion and Conclusions

Following the measurement and analysis techniques used in two previous large-area surveys of the Arctic [*Doherty et al.*, 2010; *Hegg et al.*, 2009, 2010] and North China [*Wang et al.*, 2013; *Zhang et al.*, 2013], we have estimated snow BC mixing ratios (C_{BC}^{est}), contributions to snow particulate absorption by non-BC impurities (f_{NBC}^{est}), and the sources of particulate light absorption in snow, for 67 sites in central midlatitude North America from January to March 2013.

We find that sites in Canada tended to have the lowest BC mixing ratios (typically ~5–35 ng g^{-1}; surface snow median 15 ng g^{-1}), with somewhat higher C_{BC}^{est} in the Pacific Northwest (typically ~5–40 ng g^{-1}; surface snow median 22 ng g^{-1}) and Intramountain Northwest (typically 10–50 ng g^{-1}; surface snow median 24 ng g^{-1}). The Northern U.S. Plains sites, directly south of the Canadian sites, were the dirtiest, with C_{BC}^{est} typically ~15–70 ng g^{-1} (surface snow median 30 ng g^{-1}); multiple sample layers in this region had >100 ng g^{-1} BC in snow.

At the Pacific Northwest sites and most Intramountain Northwest sites, almost all snow particulate absorption was due to BC (f_{NBC}^{est} ~10–30%), and this BC was from a mix of biomass and fossil fuel combustion (Figure 9). At these sites, the non-BC absorber is likely predominantly organic "brown" carbon [*Andreae and Gelencsér*, 2006]. However, for some Intramountain Northwest sites, up to 50% or more of absorption was due to non-BC components, and for many of the Northern U.S. Plains sites, 50–100% of absorption was due to non-BC components. Chemical and PMF analysis indicates that the non-BC absorption for most of these sites was by soil, though at some sites high mixing ratios of both soil and combustion aerosol contributed significantly to snow particulate absorption. In Canada, f_{NBC}^{est} varied from 10% to 60%, with increases in the non-BC fraction of absorption correlating ($r^2 = 0.35$) with an increasing contribution to absorption by soil (F_{SOIL}). At the U.S. sites where soil had a strong influence, the snow tended to be thin and patchy. The finding of a significant soil contribution to absorption at some Canadian sites (especially the more northern Canadian sites) is somewhat

©2014. American Geophysical Union. All Rights Reserved.

surprising, given the greater snow cover and snow depth (Figure 6). Conceivably, this is due to longer-range transport of soil to the study region. As at the Pacific Northwest sites, where biomass and fossil fuel combustion were the primary source of snow particulate absorption, f_{NBC}^{est} is ~10–30%.

Newly fallen (<3 day old, and often <1 day old) snow samples were collected at many sites. While in some cases newly fallen snow was cleaner than snow the snowpack at that site or than in the region generally (e.g., at sites 30–34), new snow was not systematically cleaner than old snow. In the U.S. Great Plains, in particular, we suspect that the snow deposited to the surface was mixed with blowing soil within a few or a few tens of meters of the surface. This makes it difficult to compare particulate mixing ratios in newly fallen snow samples to what one would expect in a model based on, e.g., model-driven snowfall rates and atmospheric concentrations of combustion aerosol and dust based on emissions, along with modeled transport/scavenging processes. Our measurements do not allow us to separate the influence of locally blown soil versus more regionally or long-range-transported soil on our samples of newly deposited snow, so we cannot definitively quantify how much local-scale processes are influencing snow particulate absorption.

Snow in midlatitude North America was, as expected, somewhat dirtier than *Doherty et al*. [2010] found in the Arctic, where median C_{BC}^{est} was <10 ng g^{-1} for all but northern Norway (21 ng g^{-1}) and Russia (~30–40 ng g^{-1}) [*Doherty et al*., 2010, Table 2]. However, the snow sampled here was much cleaner than that in the China survey of *Wang et al*. [2013]. There, C_{BC}^{est} ranged from a regional median of >100 ng g^{-1} near the northern border of northeast China to ~300–400 ng g^{-1} in north-central China and >900 ng g^{-1} in industrial northeast China [*Wang et al*., 2013, Table 2].

In the Arctic, the fraction of particulate absorption due to non-BC constituents was typically 25–45% [*Doherty et al*., 2010], and essentially all snow particulate absorption was attributed to combustion aerosol [*Hegg et al*., 2009, 2010]. Near the North Pole (snow on sea ice) and in Greenland in summer, the combustion aerosol source was predominantly fossil fuel pollution [*Hegg et al*., 2009, 2010], with pollution also contributing significantly to some Eastern Russia sites [*Hegg et al*., 2009], but for the rest of the Arctic sites, snow particulate absorption was strongly dominated by biomass combustion. In contrast, for both northwest (desert) and north-central (great plains) sites in China, soil and mineral dust dominated snow particulate absorption, and it even played a strong role in the very polluted industrial northeast [*Zhang et al*., 2013]. The remainder of the absorption in north-central China was predominantly due to biomass/biofuel combustion. In the industrial northeast, it was attributed about equally to biomass/biofuel and industrial/urban aerosol [*Zhang et al*., 2013].

Sources of soil/dust to snow in North China are likely a mix of soil from very local sources and regionally transported desert dust [*Zhang et al*., 2013]. Regionally transported desert dust has also been shown to have a significant impact on snow albedo, snowmelt rates/timing, and snow cover in the San Juan Mountains of Colorado [e.g., *Painter et al*., 2007, 2012; *Deems et al*., 2013]. In our North American survey we found soil in snow to be a significant, and perhaps dominant, driver of reduced snow albedo in the U. S. Northern Plains region, as well as at a few sites in the Intramountain Northwest and in Canada. In northwest North Dakota oil exploration activities are likely adding both soil and elevated levels of combustion particles to the snow, producing some of the dirtiest snow (high C_{BC}^{max}; Figure 7a) and some of the highest BC mixing ratios (high C_{BC}^{est}; Figures 7b and 8a) measured in our survey. Here absorption of sunlight by non-BC components in snow is comparable to or greater than absorption by BC (compare Figures 8a and 8c). While regional- and global-scale models may capture the desert dust sources in, e.g., western China, they are unlikely to capture the very local sources of soil found to be important in both north China (particularly Inner Mongolia) and the Great Plains of North America. If this is the case, models may underestimate snow albedo reduction by dust/soil and overestimate the role of BC in snow albedo reduction over broad areas of midlatitude seasonal snow.

It is to be expected that there would be more soil in snow in years that have thinner snow cover (more exposed soil) and/or higher winds (soil more easily lofted). The 2012–2013 winter was not anomalous in snow cover, but some winters do have greater snow depth/cover (e.g., see http://www.nohrsc.noaa.gov/nsa/ for maps of historical snow depth, SWE, and other snow variables). In these years soil sources will likely play a less dominant role in snow albedo reduction. Anecdotally, in the U.S. Northern Plains region, we noted that where there were adjacent tilled and untilled agricultural fields and thin snow cover, the tilled fields were often snow free whereas the untilled fields still had snow cover. We expect this is due to two factors: First, the

©2014. American Geophysical Union. All Rights Reserved.

stubble acts as a wind block (like a snow fence), so snow is captured between stubble rows, whereas it simply blows across tilled fields and does not get captured as readily in small drifts. Second, the disturbed soil on the tilled fields was more easily lofted and mixed in with snow, darkening the snow and making it sublimate and/or melt sooner. Thus, snow cover in some locations may be more strongly driven by local farming practices than by, e.g., BC emissions.

Integration of a subset of the 2013 midlatitude measurements presented here with data from 2007 and 2009 surveys into Arctic Canada shows a decrease in snow BC mixing ratios with latitude, as well as a shift in the sources of the absorbing particles. At the 2013 sites, pollution, soil, and biomass combustion all contribute significantly to absorption. While we did not find a latitudinal gradient in F_{SOIL} within the 2013 data set (which was confined to <57°N), for Canadian sites at higher latitudes (64°N–77°N), a PMF analysis attributed no absorption to soil and nearly all absorption is due to biomass/biofuel combustion.

As in previous surveys, significant variations in snow particulate mixing ratios were found within a given region, at different snow depths at a given sampling site, and in side-by-side (<1 m separation) snow profiles. These findings emphasize the need for the collection of multiple sample profiles at many sampling sites within a given region in order for measurements to be regionally representative. This is particularly true for sites close to sources: Both the present survey and an earlier survey showed much greater spatial/depth variations in snow particulate mixing ratios at lower latitudes than at higher latitudes in North America (see Figure 10 and in *Doherty et al*. [2010] results for Canadian sub-Arctic and Arctic regions). At the more local scale, three transections of newly fallen snow samples at a range of distances from Billings, Montana, Grand Forks, North Dakota, and Calgary, Alberta, showed BC mixing ratios increasing by a factor of about 2 to 4 within a few tens of kilometers of the cities.

In addition to the analyses of snow samples, soil samples were collected at most sampling sites with the primary goal of measuring their absorption Ångström exponent so that we could separate snow particulate absorption due to soil and nonsoil constituents. $\mathring{A}_{soil}$ varied from 2.5 to 6.5. It was somewhat higher in the Pacific Northwest, Rockies, and drier Great Plains sites (typically ~3–5) than at the wetter Great Plains sites (more vegetation cover in summer; more snow cover in winter) and all sites in Canada (typically ~2–4). Sites 19 and 20, in the dry basins of Wyoming, had notably higher $\mathring{A}_{soil}$ (6.6 and 6.2). Soil samples were collected and analyzed using the same techniques in the north China study of *Wang et al*. [2013]. Collectively, this database of $\mathring{A}_{soil}$ (Tables 2–5 herein and Table 1 of *Wang et al*. [2013]) may be of utility for other efforts, such as remote sensing of atmospheric aerosol.

Acknowledgments
This research project was funded by EPA STAR grant RD-82503801. This publication was funded in part by the Joint Institute for the Study of the Atmosphere and Ocean (JISAO) under NOAA Cooperative agreement NA10OAR4320148 and is JISAO contribution 2285. We thank Ariana Samuelson for assistance with ISSW measurements. R. Zhang acknowledges support from the China Scholarship Fund. We warmly thank the many farmers in the U.S. and Canada who granted us access to their property to sample snow, usually with a bit of perplexity but always with a great deal of friendliness and an offer for us to "take all the snow you want!". The full data set from this study is available by emailing the lead author (sarah-d@atmos.washington.edu) or by downloading it from www.atmos.washington.edu/articles/BC_LAP_Snow_FieldData/.

References

Andreae, M. O., and A. Gelencsér (2006), Black carbon or brown carbon? The nature of light-absorbing carbonaceous aerosols, *Atmos. Chem. Phys.*, *6*, 3131–3148, doi:10.5194/acp-6-3131-2006.

Bond, T. C., and R. W. Bergstrom (2006), Light absorption by carbonaceous particles: An investigative review, *Aerosol Sci. Technol.*, *40*(1), 27–67.

Bond, T. C., et al. (2013), Bounding the role of black carbon in climate: A scientific assessment, *J. Geophys. Res. Atmos.*, *118*, 5380–5552, doi:10.1002/jgrd.50171.

Chen, L. W. A., J. G. Watson, J. C. Chow, and K. L. Magliano (2007), Quantifying $PM_{2.5}$ source contributions for the San Joaquin valley with multivariate receptor models, *Environ. Sci. Technol.*, *41*, 2818–2826.

Clarke, A. D., and K. J. Noone (1985), Soot in the Arctic snowpack: A cause for perturbations in radiative transfer, *Atmos. Environ.*, *19*, 2045–2053.

Dang, C., and D. A. Hegg (2014), Quantifying light absorption by organic carbon in western North American snow by serial chemical extractions, *J. Geophys. Res. Atmos.*, *19*, 10,247–10,261, doi:10.1002/2014JD022156.

Deems, J. S., T. H. Painter, J. J. Barsugli, J. Belnap, and B. Udall (2013), Combined impacts of current and future dust deposition and regional warming on Colorado River Basin snow dynamics and hydrology, *Hydrol. Earth Syst. Sci.*, *17*, 4401–4413, doi:10.5194/hess-17-4401-2013.

Doherty, S. J., S. G. Warren, T. C. Grenfell, A. D. Clarke, and R. E. Brandt (2010), Light-absorbing impurities in Arctic snow, *Atmos. Chem. Phys.*, *10*, 11,647–11,680, doi:10.5294/acp-10-11647-2010.

Draxler, R. R., and G. D. Rolph (2012), HYSPLIT (Hybrid Single-Particle Lagrangian Integrated Trajectory) model. ARL Air Resources Laboratory. [Available at http://ready.arl.noaa.gov/HYSPLIT.php.]

Eldred, R. A., T. A. Cahill, and R. G. Flocchini (1997), Composition of $PM_{2.5}$ and PM_{10} aerosols in the IMPROVE network, *J. Air Waste Manage.*, *47*, 194–203.

Environmental Protection Agency (2000), Frequent, routine flaring may cause excessive, uncontrolled sulfur dioxide releases. Office of Enforcement and Compliance Assurance Enforcement Alert, EPA 300-N-00-014. [Available at www.epa.gov/oeca/ore/enfalert.]

Flanner, M. G., C. S. Zender, J. T. Randerson, and P. J. Rasch (2007), Present-day climate forcing and response from black carbon in snow, *J. Geophys. Res.*, *112*, D11202, doi:10.1029/2006JD008003.

Flanner, M. G., C. S. Zender, P. G. Hess, N. M. Mahowald, T. H. Painter, V. Ramanathan, and P. J. Rasch (2009), Springtime warming and reduced snow cover from carbonaceous particles, *Atmos. Chem. Phys.*, *9*, 2481–2497, doi:10.5194/acp-9-2481-2009.

Gao, S., D. A. Hegg, P. V. Hobbs, T. W. Kirchstetter, B. I. Magi, and M. Sadelik (2003), Water-soluble organic compounds in aerosols associated with savanna fires in southern Africa: Identification, evolution and distribution, *J. Geophys. Res.*, *108*(D13), 8491, doi:10.1029/2002JD002324.

©2014. American Geophysical Union. All Rights Reserved.

Garrett, T. J., C. Zhao, and P. C. Novelli (2010), Assessing the relative contributions of transport efficiency and scavenging to seasonal variability in Arctic aerosol, *Tellus B*, *62*(3), 190–196, doi:10.1111/j.1600-0889.2010.00453.x.

Grenfell, T. C., S. J. Doherty, A. D. Clarke, and S. G. Warren (2011), Spectrophotometric determination of absorptive impurities in snow, *Appl. Opt.*, *50*(14), 2037–2048.

Hagler, G. S. W., M. H. Bergin, E. A. Smith, and J. E. Dibb (2007a), A summer time series of particulate carbon in the air and snow at Summit, Greenland, *J. Geophys. Res.*, *112*, D21309, doi:10.1029/2007JD008993.

Hagler, G. S. W., M. H. Bergin, E. A. Smith, J. E. Dibb, C. Anderson, and E. J. Steig (2007b), Particulate and water-soluble carbon measured in recent snow at Summit, Greenland, *Geophys. Res. Lett.*, *34*, L16505, doi:10.1029/2007GL030110.

Hegg, D. A., S. G. Warren, T. C. Grenfell, S. J. Doherty, T. V. Larson, and A. D. Clarke (2009), Source attribution of black carbon in snow, *Environ. Sci. Technol.*, *43*(11), 4016–4021, doi:10.1021/es803623f.

Hegg, D. A., S. G. Warren, T. C. Grenfell, S. J. Doherty, and A. D. Clarke (2010), Sources of light absorbing aerosol in arctic snow and their seasonal variability, *Atmos. Chem. Phys.*, *10*, 10,923–10,938, doi:10.5194/acp-10-10923-2010.

Huang, J., Q. Fu, W. Zhang, X. Wang, R. Zhang, H. Ye, and S. Warren (2011), Dust and black carbon in seasonal snow across northern China, *Bull. Am. Meteorol. Soc.*, *92*, 175–181, doi:10.1175/2010BAMS3064.1.

Ite, A. E., and U. J. Ibok (2013), Gas flaring and venting associated with petroleum exploration and production in Nigeria's delta, *Am. J. Environ. Prot.*, *1*(4), 70–77, doi:10.12691/env-1-4-1.

Jacobson, M. Z. (2004), Climate response of fossil fuel and biofuel soot, accounting for soot's feedback to snow and sea ice albedo and emissivity, *J. Geophys. Res.*, *109*, D21201, doi:10.1029/2004JD004945.

Koch, D., et al. (2009a), Evaluation of black carbon estimations in global aerosol models, *Atmos. Chem. Phys.*, *9*(22), 9001–9026, doi:10.5194/acp-9-9001-2009.

Koch, D., S. Menon, A. Del Genio, R. Ruedy, I. Alienov, and G. A. Schmidt (2009b), Distinguishing aerosol impacts on climate over the past century, *J. Clim.*, *22*(10), 2659–2677, doi:10.1175/2008jcli2573.1.

LaChapelle, E. R. (1969), *Field Guide to Snow Crystals*, Univ. of Wash. Press, Seattle.

Lavoué, D., C. Liousse, and H. Cachier (2000), Modeling of carbonaceous particles emitted by boreal and temperate wildfires at northern latitudes, *J. Geophys. Res.*, *105*(D22), 26,871–26,890, doi:10.1029/2000JD900180.

Leck, C., J. Heintzenberg, and M. Engard (2002), A meridional profile of the chemical composition of submicrometre particles over the East Atlantic Ocean: Regional and hemispheric variables, *Tellus B*, *54*, 377–394.

Malm, W. C., J. F. Sisler, D. Huffman, R. A. Eldred, and T. A. Cahill (1994), Spatial and seasonal trends in particle concentration and optical extinction in the United States, *J. Geophys. Res.*, *99*(D1), 1347–1370, doi:10.1029/93JD02916.

McConnell, J. R., R. Edwards, G. L. Kok, M. G. Flanner, C. S. Zender, E. S. Saltzman, J. R. Banta, D. R. Pasteris, M. M. Carter, and J. D. W. Kahl (2007), 20th-century industrial black carbon emissions altered Arctic climate forcing, *Science*, *317*(5843), 1381–1384, doi:10.1126/science.1144856.

Paatero, P. (1997), Least squares formulation of robust non-negative factor analysis, *Chemom. Intell. Lab.*, *37*, 23–35.

Paatero, P., and U. Tapper (1993), Analysis of different modes of factor analysis as least-squares fit problems, *Chemometr. Intell. Lab.*, *18*, 183–194.

Paatero, P., and U. Tapper (1994), Positive matrix factorization: A nonnegative factor model with optimal utilization of error estimates of data values, *Environmetrics*, *5*, 111–126.

Paatero, P., P. K. Hopke, J. Hoppenstock and S. I. Eberly (2003), Advanced factor analysis of spatial distributions of $PM_{2.5}$ in the eastern United States, *Environ. Sci. Technol.*, *37*, 2460–2476, doi:10.1021/es0261978.

Painter, T. H., A. P. Barrett, C. C. Landry, J. C. Neff, M. P. Cassidy, C. R. Lawrence, K. E. McBride and G. L. Farmer (2007), Impact of disturbed desert soil on duration of mountain snow cover, *Geophys. Res. Lett.*, *34*, L12502, doi:10.1029/2007GL030284.

Painter, T. H., S. M. Skiles, J. S. Deems, A. C. Bryant, and C. C. Landry (2012), Dust radiative forcing in snow on the Upper Colorado River Basin: 1. A 6 year record of energy balance, radiation and dust concentrations, *Water Resour. Res.*, *48*, W07521, doi:10.1029/2012WR011985.

Pikelnaya, O., J. H. Flynn, C. Tsai, and J. Stutz (2013), Imaging DOAS detection of primary formaldehyde and sulfur dioxide emissions from petrochemical flares, *J. Geophys. Res. Atmos.*, *118*, 8716–8728, doi:10.1002/jgrd.50643.

Potter, J. G. (1965), *Snow Cover, Climatological Studies Number 3*, 69 pp., Canada Dep. of Transp., Toronto, Canada.

Qian, Y., W. I. Gustafson, L. R. Leung and S. J. Ghan (2009), Effects of soot-induced snow albedo change on snowpack and hydrological cycle in western United States based on Weather Research and Forecasting chemistry and regional climate simulations, *J. Geophys. Res.*, *114*, D03108, doi:10.1029/2008JD011039.

Reff, A., S. I. Eberly, and P. V. Bhave (2007), Receptor modeling of ambient particulate matter data using positive matrix factorization: Review of existing methods, *J. Air Waste Manage. Assoc.*, *57*, 146–154.

Schwarz, J. P., J. R. Spackman, R. S. Gao, L. A. Watts, P. Stier, M. Schulz, S. M. Davis, S. C. Wofsy, and D. W. Fahey (2010), Global-scale black carbon profiles observed in the remote atmosphere and compared to models, *Geophys. Res. Lett.*, *37*, L18812, doi:10.1029/2010GL044372.

Schwarz, J. P., S. J. Doherty, G. L. Kok, F. Li, S. T. Ruggiero, C. E. Tanner, A. E. Perring, R. S. Gao, and D. W. Fahey (2012), Assessing Single Particle Soot Photometer and Integrating Sphere/Integrating Sandwich Spectrophotometer measurement techniques for quantifying black carbon concentration in snow, *Aerosol Meas. Tech.*, *5*, 2581–2592, doi:10.5194/amt-5-2581-2012.

Schwarz, J. P., R. S. Gao, A. E. Perring, J. R. Spackman, and D. W. Fahey (2013), Black carbon aerosol size in snow, *Nat. Sci. Rep.*, *3*, 1356, doi:10.1038/srep01356.

Wang, X., S. J. Doherty, and J. Huang (2013), Black carbon and other light-absorbing impurities in snow across Northern China, *J. Geophys. Res. Atmos.*, *118*, 1471–1492, doi:10.1029/2012JD018291.

Warren, S. G., and W. J. Wiscombe (1980), A model for the spectral albedo of snow. II: Snow containing atmospheric aerosols, *J. Atmos. Sci.*, *37*, 2734–2745.

Xu, B., J. Cao, D. R. Joswiak, X. Liu, H. Zhou, and J. He (2012), Post-depositional enrichment of black soot in snow-pack and accelerated melting of Tibetan glaciers, *Environ. Res. Lett.*, *7*, doi:10.1088/1748-9326/7/1/014022.

Yan, G., H.-M. Cho, I. Lee, and G. Kim (2012), Significant emissions of ^{210}Po by coal burning into the urban atmosphere of Seoul, Korea, *Atmos. Environ.*, *54*, 80–85, doi:10.1016/j.atmosenv.2012.02.090.

Ye, H., R. D. Zhang, J. S. Shi, J. P. Huang, S. G. Warren, and Q. Fu (2012), Black carbon in seasonal snow across northern Xinjiang in northwestern China, *Environ. Res. Lett.*, *7*, 044002, doi:10.1088/1748-9326/7/4/044002.

Zhang, R., D. A. Hegg, J. Huang, and Q. Fu (2013), Source attribution of insoluble light-absorbing particles in seasonal snow across northern China, *Atmos. Chem. Phys.*, *13*, 6091–6099, doi:10.5194/acp-6091-2013.

©2014. American Geophysical Union. All Rights Reserved.

Erratum

In the originally published version of this article, the results of a coding error were discovered in the first block of entries in Table 6. The errors have since been corrected, and this version may be considered the authoritative version of record.

©2014. American Geophysical Union. All Rights Reserved.